

# INTRODUCING NANOVALVE TECHNIQUE FOR NATURAL GAS STORAGE

by  
Kirby L. Tate

A thesis submitted to the Faculty and the Board of Trustees of the Colorado School of Mines in partial fulfillment of the requirements for the degree of Master of Science (Chemical and Biological Engineering).

Golden, Colorado

Date \_\_\_\_\_

Signed: \_\_\_\_\_

Kirby L. Tate

Signed: \_\_\_\_\_

Dr. Moises A. Carreon

Thesis Advisor

Signed: \_\_\_\_\_

Dr. David M.W. Marr

Department Head

Chemical and Biological Engineering

## ABSTRACT

In order for natural gas vehicles to be economically feasible in residential consumer sector, the limitations of the current natural storage approaches (Compressed Natural Gas and Liquefied Natural Gas) must be overcome. Advances in the Adsorbed Natural Gas storage approach have been made, however, these advances do not fit within the parameters (storage pressure of 35 bar) set by Advanced Research Projects Agency-Energy (ARPA-E) of the U.S. Department of Energy (DOE). The research presented here establishes a novel technique to effectively store methane. This nanovalved technique involves loading a pelleted adsorbent at high pressure, sealing a layer coated on the adsorbent pellet, and reducing the storage vessel to a low pressure. Using zeolite 5A beads as a model adsorbent and MCM-48 as a nanovalving layer, >50% of the maximum methane capacity of zeolite 5A (73 V/V) was able to be maintained after being reduced to a pressure of 1 bar. After establishing the feasibility of the nanovalving technique with MCM-48, again using zeolite 5A beads as a model adsorbent, the impact of coordinating metal of MOF nanovalve layers was assessed. This study was to aid in designating material properties of the nanovalving layer that allow for better sealing and better performance. Aluminum was established as a desirable component in the nanovalving layer (two layers of Al-MOF on zeolite 5A beads was able to maintain 46% of the maximum methane capacity). The work herein illustrates the nanovalving technique can store a high percentage of loaded methane at low pressure. With a high methane capacity adsorbent and an optimized nanovalving layer, the possibility of achieving the storage targets set by ARPA-E is promising.

## TABLE OF CONTENTS

ABSTRACT .....	iii
LIST OF FIGURES.....	vi
LIST OF TABLES.....	viii
CHAPTER 1: NATURAL GAS STORAGE .....	1
1.1 BACKGROUND.....	2
1.1.1 COMPRESSED NATURAL GAS (CNG).....	2
1.1.2 LIQUEFIED NATURAL GAS (LNG).....	2
1.1.3 ADSORBED NATURAL GAS (ANG) .....	3
1.2 MOTIVATION .....	4
CHAPTER 2: LITERATURE REVIEW.....	6
2.1 ZEOLITES .....	6
2.2 CARBONS.....	7
2.3 METAL ORGANIC FRAMEWORKS (MOFs) AND COVALENT ORGANIC FRAMEWORKS (COFs) .....	8
2.4 SUMMARY AND JUSTIFICATION.....	11
CHAPTER 3: ZEOLITE ADSORBENT- MCM48 NANOVALVES FOR CH4 STORAGE.....	13
CHAPTER 4: ZEOLITE ADSORBENT-MOF LAYERED NANOVALVES FOR CH4 STORAGE.....	21

CHAPTER 5: CONCLUSIONS AND RECCOMENDATIONS.....	31
REFERENCES.....	34
APPENDIX A.....	39
APPENDIX B.....	57

## LIST OF FIGURES

Figure 3.1 (a) Diagram of CH <sub>4</sub> storage by using nanovalved adsorbents; (b) cross-sectional SEM image of MCM-48-5A (EDS analysis points are indicated in the figure); (c) HRTEM images and pore sizes of MCM-48-5A adsorbent; (d) HRTEM image and pore size of MLD-MCM-48-5A adsorbent. ....	15
Figure 3.2 Steady state CH <sub>4</sub> storage capacity of MCM-48 coated 5A adsorbent calcined at different temperatures and uncoated 5A zeolite. ....	17
Figure 3.3 Three cycles of CH <sub>4</sub> storage test on MLD-MCM-48-5A adsorbent (loading pressure 50 bar, storage pressure 1 bar).....	19
Figure 3.4 Comparison of nanovalve adsorbents with porous materials for CH <sub>4</sub> storage: CH <sub>4</sub> storage amount versus CH <sub>4</sub> storage pressure. Blue squares and triangles (1-8) represent porous materials from the literature; <sup>9,18,25-27</sup> bulk density of methane is represented by black square and triangle (9); red squares (10-11) indicate nanovalve adsorbents from this study.....	19
Figure 4.1 XRD patterns of the as-synthesized crystals (a) HKUST-1 (b) GaMOF (c) AlMOF and (d) CoMOF. Peak indexes are from Lin <i>et al</i> <sup>21</sup> .....	23
Figure 4.2 XRD for crushed (a) bare zeolite 5A beads and crushed 2-layer samples of (b) AlMOF (c) GaMOF (d) CoMOF and (e) HKUST-1 on zeolite 5A beads. MOF peaks are indexed from Lin <i>et al</i> <sup>21</sup> . ....	42
Figure 4.3 Nanovalve performance data obtained by in-house adsorption apparatus. The samples were degassed under vacuum for 2 hours and then loaded with methane to a pressure of 50 bar. The nanovalves were sealed by flow ethanol carried by methane at 50bar for 2 hours. After venting to ambient pressure, leak pressure was recorded for 48 hours before obtaining the final amount stored. ....	27
Figure 4.4 SEM images of 2-layers of (a) AlMOF (b) GaMOF (c) CoMOF and (d) HKUST-1 on zeolite 5A beads. The thicknesses for the MOF layers were Co-MOF ~7.5µm, Al-MOF ~10.5µm, Ga-MOF ~15.5µm, and HKUST-1 ~27.5µm. ....	28
Figure A1 Nanovalve testing apparatus. ....	40

Figure A2	Storage pressure data for 1-layer GaMOF depicting stabilization well within 48hours. ....	56
Figure A3	SEM of (a)1-layer AlMOF, (b) 2-layer AlMOF, and (c) 3-layer AlMOF. ....	56
Figure B1	Diagram of coating procedure for MCM-48-5A adsorbent and pictures of samples.....	63
Figure B2	Adsorption isotherm of uncoated 5A zeolite beads at 20°C. ....	64
Figure B3	Nano-valved sorbent functioning testing system. 1-pressure transducer, 2-adsorption tank, 3-reference cell, MFC-mass flow controller, R1-back pressure regulator, V1-V8 valve.....	65
Figure B4	CH <sub>4</sub> storage test (loading pressure 50 bar, storage pressure 1bar) on MCM-48-5A adsorbent calcined at 350°C (a); calcined at 400°C (b); calcined at 450°C; uncoated 5A zeolite (d). ....	66
Figure B5	HRTEM images and pore sizes of MCM-48-5A adsorbents. ....	67
Figure B6	HRTEM images and pore sizes of MLD-MCM-48-5A adsorbents.....	68

## LIST OF TABLES

Table 2.1	Notable Zeolites and Corresponding Methane Uptakes at 500psig and 298K .....	6
Table 2.2	Methane Uptakes for Various Types of Carbon at ~35bar and 298K .....	8
Table 2.3	Methane Uptake for MOFs and COFs at 35bar and 298K. Values in parenthesis are computational values. ....	10
Table A1	Legend for nanovalve testing apparatus. ....	41
Table A2	BET surface area of the control and the four 2-layer nanovalve samples. ....	57
Table A3	EDX of HKUST-1 as-synthesized crystals. ....	57
Table B1	Atomic EDS analysis for MCM-48-5A. ....	62
Table B2	BET area before and after MCM-48 coating. ....	62
Table B3	Energy densities of sorbents at 25°C with loading pressures of 250 and 300 bar .....	62

## CHAPTER 1

### NATURAL GAS STORAGE

The United States is the world's largest producer of natural gas<sup>1,2</sup>. As of 2015, the United States is producing 28.8 trillion cubic feet of natural gas per year<sup>3</sup>. The United States natural gas production has been increasing every year since 2010<sup>3</sup> and this increase in production can, in part, be contribution to the increasing use of fracking and other technologies that release previously untapped natural gas in shale<sup>4</sup>. In fact, the United States was producing so much natural gas in 2011 that United States producers were filing bankruptcy. To stabilize natural gas prices by increasing the United States natural gas consumption, Congress passed a bill to open natural gas export to Japan<sup>5</sup>.

While decrease in price of natural gas has caused trouble in the financial state of industries in natural gas production, consumers are seeing a widening gap in price between crude oil and natural gas. Crude oil prices are hovering around \$20/MMBtu while natural gas prices are hovering around \$2/MMBtu.<sup>6</sup>

Not only is natural gas abundant and inexpensive, natural gas is also cleaner burning than gasoline. It has been demonstrated that when vehicles run on natural gas, on average, 86% less CO, 26% less CO<sub>2</sub>, and 77% less NO<sub>x</sub> are emitted as compared to gasoline run vehicles.<sup>7</sup> The global temperature has been increasing at a rate that is uncharacteristic of natural fluctuations, and is projected to increase 0.1°C to 0.2°C which is an increase more than that of the last 10,000 years.<sup>8</sup> To mitigate human impact on the global temperature increase, cleaner burning fuels for vehicles are being investigated. Natural gas lends itself as an alternative vehicular fuel source because it

is abundant, inexpensive, and clean burning. However, the biggest hindrance to natural gas vehicles is a suitable onboard storage technology.

## 1.1 Background

The three main approaches to natural gas (major component being methane) storage: Compressed Natural Gas (CNG), Liquefied Natural Gas (LNG), and Adsorbed Natural Gas (ANG). The advantages and disadvantages of each method of storage are discussed in the next paragraphs.

### 1.1.1 Compressed Natural Gas (CNG)

CNG storage technology, as the name implies, relies on keeping the natural gas under high pressure in the storage vessel. Typically, this pressure is 3000 psig<sup>9</sup> (200 bar) or 300 bar<sup>10,11</sup>. The advantage of this technique lies in its simplicity and effectiveness. However, to achieve these elevated pressures, expensive, multi-stage compressors and metering equipment are required.<sup>9</sup> To accommodate a reasonable onboard storage amount, heavy, cumbersome cylinders and onboard compressors must also be incorporated in the vehicle—taking up considerable space.<sup>12</sup> Even with all the equipment and space needed to house CNG technology for onboard storage, CNG is only able to achieve ~25% of the energy density of gasoline (energy density of gasoline being 32.4 MJ/L).<sup>13,14</sup> Because the space necessary to board the storage vessels and compression equipment is so large, it is unlikely that the CNG storage approach be used outside the commercial sector.

### 1.1.2 Liquefied Natural Gas (LNG)

The LNG storage approach does not require high pressure, but rather extremely low temperatures. Typically, the natural gas must be cooled to and kept at 113K.<sup>10,11</sup> In

order to keep such low temperatures, cryogenic tanks with thick insulation are required. Refueling stations using this type of storage would likely require specialist to ensure the refueling process is safe.<sup>15</sup> Because LNG storage requires intermittent venting due to boil off, long term storage using LNG technology is an issue. The production of LNG is expensive, however, it is able to achieve ~64% of the energy density of gasoline.<sup>13</sup> The expense and longevity of storage make it likely that the LNG storage approach not leave the commercial and transport sectors.

### 1.1.3 Adsorbed Natural Gas (ANG)

The ANG storage approach involves physically or chemically attaching (adsorption) methane molecules onto a solid material. How much methane can be adsorbed and at what pressure and temperature is a property of the material itself. This has led to increased interest in high surface area adsorbents such as zeolites,<sup>16–18</sup> metal-organic frameworks (MOFs),<sup>17,19,20</sup> covalent organic frameworks (COF),<sup>21–23</sup> activated carbon,<sup>17,24</sup> and carbon nanotubes.<sup>25,26</sup> Interest in methane storage using activated carbon and carbon nanotubes started in the early 1990s.<sup>27,28</sup> Activated carbon was promising in that it could ideally adsorb methane with a similar energy density to CNG technology. However, with the discovery of HKUST-1 in 1999,<sup>29</sup> it was found that MOFs could surpass the methane uptake capacities of carbons and zeolites. MOFs consisting of one or more coordinating metal combined with one or more organic ligands to form periodic, crystalline frameworks, allow for a seemingly endless number of possible frameworks.<sup>30,31</sup> Because experimental research on such a large number of materials is so daunting, computational researchers have taken on the task to provide insight as to which MOFs<sup>30,32,33</sup> and COFs<sup>34</sup> are most promising for adsorbent

candidates.

Recently, a list of MOFs most likely to be able to fulfill the target set by the Advanced Research Projects Agency-Energy (ARPA-E) of the U.S. Department of Energy (DOE) of a volumetric capacity of 315 L(STP)/L sorbent (12.5 MJ/L sorbent) and gravimetric capacity of 0.5 g CH<sub>4</sub>/g sorbent<sup>16-18</sup> was compiled<sup>35</sup> using the work of Mason et al<sup>13</sup> and Furukawa et al<sup>20</sup>. The compiled list indicates that MOF-519, MOF-177, Ni-MOF-74, and HKUST-1 are at the top of the current MOF list to pursue for further research in ANG technology.

## 1.2 Motivation

Although the above mentioned materials are near or similar to the target set by ARPA-E, typically the target is met above the target's set pressure (35 bar). Typically, an adsorbent material's capacity increases with increasing methane pressure until a pressure at which the material reaches saturation. The methane saturation pressures of the above mentioned MOF materials is above the target pressure of 35 bar. Because the materials are capable of storing more methane at higher pressures, a new method, or rather a subset of the ANG approach, has been developed by Carreon, Yu and Li's group<sup>36</sup> which will be described and presented here.

This new method has been designated as the "nanovalve" storage approach due to the nature of the method. The nanovalve storage approach involves coating an adsorbent material in pellet form (herein, zeolite 5A beads) with another material (herein, MCM-48 and HKUST-1 and its derivatives). The nature of the layer of material coated on the adsorbent pellet is such that it is porous and capable of forming a continuous layer around the material. Because the layer is porous, methane is able to penetrate

through the layer and be adsorbed in the pelleted material at high pressure (herein, 50 bar). Once methane has adsorbed on the pelleted material, the pores in the layer coated on the pellet can be closed (similar to the closing of a valve). Once the pores have been closed, the pressure can be reduced to atmosphere. To reopen the pores, the sample is heated to release the stored. The hypothesis tested and described herein, involves the performance and limits of the nanovalue technique. To test the nanovalue samples, an in-house, lab-scale apparatus was designed and built (for a diagram of the in-house apparatus and more detailed procedure, see Appendix A).

## CHAPTER 2

### LITERATURE REVIEW

In the next few sections, the scope of current ANG technology will be reviewed. Specifically, the capabilities of zeolites, activated carbon, carbon nanotubes, MOFs, and COFs to adsorb natural gas (methane) will be discussed.

#### 2.1 Zeolites

Zeolites are crystalline materials made up of silicon, aluminum, and balancing ions (typically Group 1 or 2 metals).<sup>37</sup> These materials have been of interest for natural gas storage because of their chemical and mechanical stability as well as their high surface area. Notable zeolites include: zeolite 5A, 13X, 4A, MY (where M is Na, Ca, Mg, Sr, Ba), and MX (where M is Na, Ca, Mg, Sr, Ba).<sup>38-44</sup>

The above mentioned zeolites have had methane adsorption experiments conducted at 500psig (~35bar) and 298K. The methane uptakes in grams of methane per gram of sorbent at 500psig and 298K for the highest adsorbing zeolite in each category have been arranged in Table 2.1 below.

Table 2.1 Notable Zeolites and Corresponding Methane Uptakes at 500psig and 298K

Type	Methane Uptake (g/g)	Reference
5A	0.050	[38]
13X	0.053	[38]
CaX	0.082	[42]

Table 2.1 (cont'd)

Type	Methane Uptake (g/g)	Reference
BaX	0.067	[42]
CaY	0.063	[43]
MgY	0.062	[43]

## 2.2 Carbons

There are several types of carbons that are of interest in storing method, however, the two primary categories of carbons include: activated carbon (granular powder, shaped monolith, activated fiber)<sup>45–50</sup> and carbon nanotubes<sup>25,26</sup>.

Activated carbon is a material in which a carbon source has been heated and treated to leave behind stable, high surface area, non-crystalline material. Carbon nanotubes are an allotrope of carbon (like graphite, graphene, etc.) in which carbon molecules have been arranged in a cylindrical shape of high length to diameter ratio (leading to increased surface area among other properties). Table 2.2 illustrates methane uptakes at ~35 bar and 298K for various types of carbons.

Table 2.2 does not include the surface areas of each material, however, the strong correlation between increasing surface area of carbons and increasing methane uptake has been shown.<sup>15</sup> The Maxsorb with the highest methane uptake (0.211 wt%, ~109 v/v) also has the highest surface area of all the materials listed. Therefore, carbon materials are limited in methane capacity by the ability to increase the surface areas.

Table 2.2 Methane Uptakes for several types of Carbons at ~35bar and 298K

Type	Methane Uptake (g/g)	Reference
Amoco GX-32 (granular powder)	0.175	[46]
Maxsorb (Grade 30-SPP and Lot 92-05) (Kansai coke based) (granular powder)	0.211	[45]
Electrosynthesis EL (granular powder)	0.170	[45]
PX-21, Amoco (Maxsorb) (granular powder)	0.177	[47]
Saran A carbon, 36X-42.5% w/l (shaped monolith)	0.130	[48]
Saran A carbon, 12X-17.9% w/l Saran (shaped monolith)	0.113	[48]
KF 1500 (Cellulose based, Toyobo Co.) (activated fiber)	0.083	[49]
Multi-walled Carbon Nanotubes	0.008	[50]
Multi-walled Carbon Nanotubes (Alkali treatment + mixed acid treatment + mechanical shearing)	0.117	[26]
Multi-walled Carbon Nanotubes (Mechanical shearing + alkali treatment + mixed acid treatment + mechanical shearing)	0.097	[26]

### 2.3. Metal Organic Frameworks (MOFs) and Covalent Organic Frameworks (COFs)

Metal organic frameworks (MOFs) are typically crystalline materials in which the framework of the crystalline structure is formed by a metal cation coordinating with an organic ligand.<sup>30,31</sup> The coordinating metals are typically aluminum or period four

transition metals, but are not limiting to these. The organic ligand can be various compounds but typically contain electron lone pairs to coordinate with the metal cation (thus carboxylic groups, amine groups, imidazole groups, benzene groups, etc are common in the organic ligand compounds). Studies on the most promising MOFs for methane storage have been conducted.<sup>13,20,35,51</sup>

Covalent organic frameworks (COFs) are similar in structure and make up to MOFs. The primary difference between MOFs and COFs is that COFs typically have carbon or boron as a coordinating metal.<sup>52</sup> This difference allows for COFs to have a lower density than MOFs because of the use of lighter metal source. The bulk of the literature concerning COFs is by way of simulation studies<sup>34,53</sup> although experimental studies have been done.<sup>22</sup>

Table 2.3 is a compilation of the highest capacity MOFs and COFs from the above mentioned experimental and computational studies (values in parenthesis indicate computational values). Though the information presented is for methane uptakes at 35bar and 298K, none of these materials are fully saturated with methane at these conditions. The information is provided in this way for direct comparison to the DOE target at 35 bar.

Table 2.3 Methane Uptake for MOFs and COFs at 35bar and 298K. Values in parenthesis from computational studies.

Type	Methane Uptake (g/g)	Methane Uptake (STP cm <sup>3</sup> /cm <sup>3</sup> )	Reference
HKUST-1	0.185	227	[51]
Ni-MOF-74	0.138	230	[13]
PCN-14	0.171	195	[13]
UTSA-20	---	184	[51]
NU-125	---	182	[51]
NU-111	---	138	[51]
AX-21	0.225	153	[20]
MOF-519	0.150	200	[35]
MOF-520	0.198	162	[35]
MOF-5	---	126	[35]
MOF-177	---	122	[35]
COF-1	0.029(0.053)	40(196)	[34],[22]
COF-5	0.110(0.090)	89(100)	[34],[22]
COF-6	0.042(0.085)	65(165)	[53],[22]
COF-8	0.088(0.090)	87(130)	[53],[22]
COF-10	0.119(0.100)	80(100)	[53],[22]
COF-102	0.312(0.185)	187(143)	[34],[22]
COF-102-Ant	(0.116)	(215)	[34]
COF-102-Ethyl-trans	(0.158)	(184)	[34]
COF-103	0.292	175	[22]

Table 2.3 (cont'd)

Type	Methane Uptake (g/g)	Methane Uptake (STP cm <sup>3</sup> /cm <sup>3</sup> )	Reference
COF-103-Ethy-trans	(0.201)	(201)	[34]
COF-105-Ethyl-trans	(0.296)	(114)	[34]
COF-108	(0.200)	(80)	[53]

## 2.4 Summary and Justification

Although zeolites, activated carbon, carbon nanotubes, MOFs, and COFs have been of interest in the area of natural gas (methane) storage, as shown in the above sections, none of the materials meet the targets set by the Advanced Research Projects Agency-Energy (ARPA-E) of the U.S. Department of Energy (DOE), which corresponds to volumetric capacity of 315 L(STP)/L sorbent (12.5 MJ/L sorbent) and gravimetric capacity of 0.5 g CH<sub>4</sub>/g sorbent.<sup>33,51,54</sup> However, in the case of MOFs, 35bar is, typically, not the pressure at which methane saturation occurs. For example, MOF-210 at 250bar has a methane uptake of 377 L(STP)/L sorbent<sup>20</sup>.

The nanovalve method shown and described hereafter, aims to load sorbents at high pressure (where the ARPA-E storage target could be met), seal in the adsorbed methane at this high pressure, and then reduce the storage pressure to near ambient while still maintaining a high methane storage amount. The work described here uses zeolite 5A beads as sorbent and various layers including MCM-48 and HKUST-1 (and isostructural MOFs). While, as seen above, zeolite 5A does not meet the ARPA-E storage target (saturation methane capacity of 73 L (STP)/L sorbent at 50bar<sup>36</sup>), zeolite

5A is a convenient model sorbent to test the performance of various layers due to making and obtaining MOF pellets being a non-trivial, expensive process. In the next two chapters, two successful examples of nanovalved adsorbents for natural gas storage are presented: (a) zeolite 5A-adsorbent- MCM48 nanovalves and (b) zeolite 5A adsorbent-MOF nanovalves.

## CHAPTER 3

### ZEOLITE ADSORBENT- MCM48 NANOVALVES FOR CH<sub>4</sub> STORAGE

The results summarized in this Chapter have been recently published by our research group.<sup>36</sup> The information shown here uses a nanoporous coating (MCM-48 mesoporous silica) on the outer surfaces of the adsorbent zeolite 5A beads to illustrate that the conceptual nanovalve functioning process shown in Figure 3.1, panel a is experimentally achievable. Zeolite 5A was chosen as the model adsorbent for this proof of concept study because zeolite 5A is commercially available in the pelleted geometry needed for the nanovalve synthesis and zeolite 5A has a moderate methane saturation capacity.

MCM-48 was coated onto the surface of the zeolite 5A beads by sol-gel process to form a high quality layer. The synthesis procedure is presented in Appendix B and a diagram of synthesis is shown in Figure B1. The prepared nanovalve sample was then calcined to free the pores of template molecules. In addition to calcination, the MCM-48-zeolite 5A nanovalves were further modified by molecular layer deposition (MLD) to reduce the pore size in the MCM-48 coating. The capability of MLD to reduce pore size has been shown previously<sup>55,56</sup> as well as in Figure 3.1 panels c and d.

For this particular study, 2,2-Dimethylbutane (DMB) was selected as the nanovalve sealing agent because its molecular size is small enough to fit inside the pores of the MCM-48 nanovalve coating, but too larger to fit inside the pores of the zeolite 5A adsorbent. The nanovalve allows high pressure inside and low pressure outside. The maximum pressure drop that the adsorbed/sealing molecule can hold can

be calculated using Young–Laplace equation and estimated to be higher than 200 bar at room temperature for a 1.5 nm pore filled with DMB (Appendix B).

A high quality coating layer is the key to the proposed nanovalved adsorbent. In this study, MCM-48 (Mobil Composition of Matter number-48) was used because it is a periodic mesoporous amorphous silica possessing long-range ordered framework with uniform mesopores.<sup>57</sup> MCM-48 is capable of forming the essential continuous layer due to its amorphous nature. Amorphous materials are able to more easily form continuous layers as opposed to crystalline materials because amorphous materials do not have issues of formation of grain boundaries, intercrystalline defects, which are detrimental for the integrity of the resultant layers. Figure 3.1 panel b shows a continuous ~7.5  $\mu\text{m}$  thick layer of MCM-48 on zeolite 5A beads. The EDX analysis shown in Table B1 confirm that there no obvious penetration of MCM-48 gel into the pores of the zeolite 5A adsorbent. BET area dropped by 19% compared with 5A zeolite after MCM-48 coating (Table B2). The methane adsorption isotherm was measured for the bare 5A zeolite beads (Figure B2) to a pressure up to 120bar. The measured isotherm was consistent with literature data at low pressure reported by Nam et al.<sup>16</sup> As seen in Figure B2, zeolite 5A is saturated at 100bar with a capacity of 2.67mmol/g. To convert the saturation capacity to volumetric density, Hg porosimetry analysis (Appendix B) was used to obtain a bulk density of 1.22g/mL for zeolite 5A beads. Thus, the corresponding volumetric density (capacity) was found to be 73 V/V.

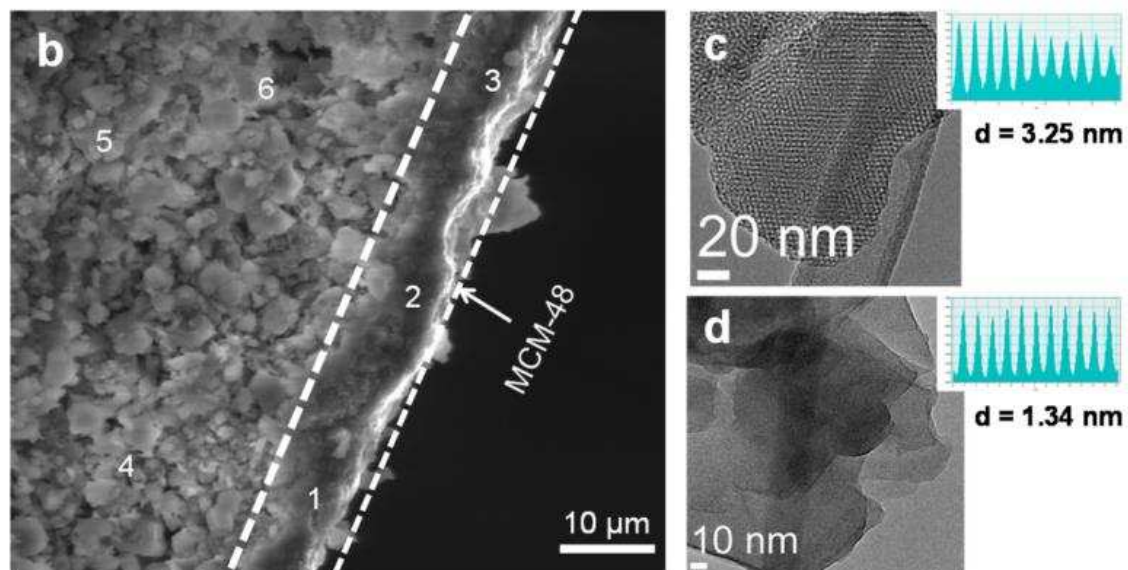
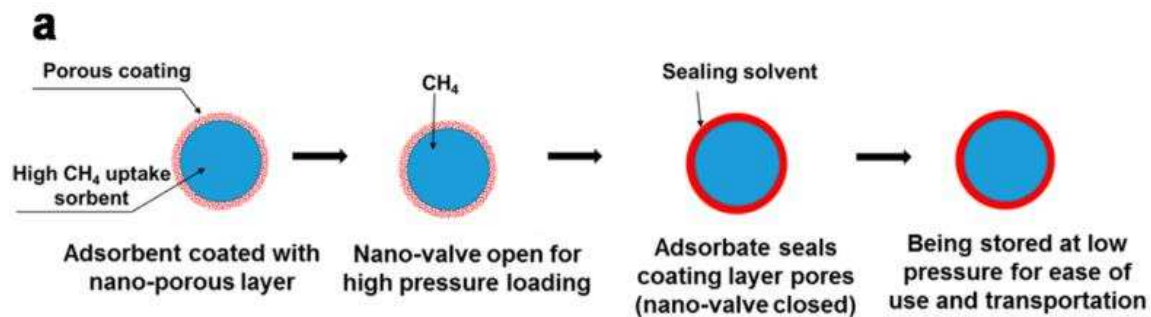


Figure 3.1. (a) Diagram of CH<sub>4</sub> storage by using nanovalved adsorbents; (b) cross-sectional SEM image of MCM-48-5A (EDS analysis points are indicated in the figure); (c) HRTEM images and pore sizes of MCM-48-5A adsorbent; (d) HRTEM image and pore size of MLD-MCM-48-5A adsorbent.<sup>36</sup>

Nanovalve functioning was tested by loading a 0.5g sample of MCM-48-zeolite 5A sample of nanovalves in to the adsorption tank (Figure B3). Methane was loaded into the sample at a pressure of 50bar. Methane was then directed to a reference filled with DMB. The DMB saturation methane was flown over the sample at 50bar for 1hour to seal the MCM-48 nanopores. The system pressure was then reduced to ~1bar and the methane stored capacity was measured as a function of time. (Full nanovalve function test procedure available in Appendix B).

As mentioned, the MCM-48 template, cetyltrimethyl- ammonium bromide (CTAB), had to be removed by calcination. Because CTAB must be removed to open the nanopores of the MCM-48 layer, the calcinations influence the nanovalve performance. Three different calcination temperatures (350, 400, and 450 °C) were investigated. As seen in Figure B4, calcination temperatures of 350 and 400 °C shown an initial methane storage of <52% of the maximum capacity of bare zeolite 5A beads after being reduced to system storage pressure (1bar) whereas a calcination temperature of 450°C shows an initial methane storage of 85%. Because MCM- 48 reduced the BET surface area of zeolite 5A by 19%, it was anticipated that the nanovalve sample would not achieve the full maximum capacity of the bare zeolite 5A beads. Higher calcination temperatures were not tested because of possible defect introduction due to thermal, and therefore, 450°C was designated as the optimal calcination condition.

Figure 3.2 shows the storage capacities at which the three calcination conditions and bare zeolite 5A reached stability (Figure B4a–c) after 4 hours at storage pressure (1bar). All three calcined samples of MCM-48-zeolite 5A samples calcined at show an

improvement in methane storage over the bare zeolite 5A (13.8 V/V, 19% of maximum) with the 350°C sample leveling at 20.9 V/V (28.7% of maximum), the 400°C sample at 23.6 V/V (32.4% of maximum), and the 450°C sample at 32.2 V/V (44.1% of maximum).

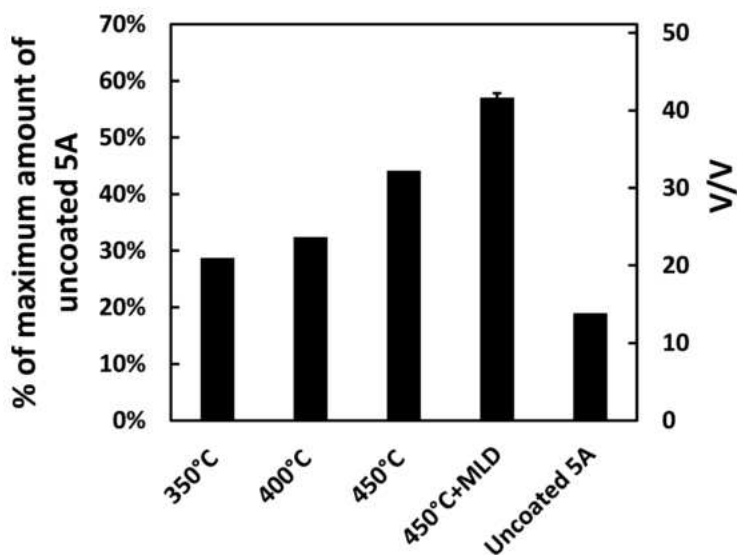


Figure 3.2. Steady state CH<sub>4</sub> storage capacity of MCM-48 coated 5A adsorbent calcined at different temperatures and uncoated 5A zeolite.<sup>36</sup>

Figure 3.1 and Figure B4 show high-resolution transmission electron microscopy (HRTEM) images of MCM-48 coated zeolite 5A adsorbent indicating expected MCM-48 pore sizes of 3.1-3.4nm. Because 3nm pores should be able to hold a pressure drop >100bar (Appendix B), the nonuniformity of the MCM-48 pore size was suspected as the reason for the decrease in methane storage from 85% to 44% for the MCM-48-zeolite 5A sample calcined at 450 °C calcination.

The nonuniformity can be improved by MLD post-treatment. MLD is a gas phase deposition technique capable of depositing ultrathin conformal coatings on high aspect ratio substrate with accurate angstrom-level coating thickness control.<sup>55,56</sup> After three

cycles of MLD (Appendix B) on the 450°C calcined MCM-48 coated zeolite 5A adsorbent (MLD-MCM-48-5A) the MCM-48 pore size was ~1.34–1.42 nm (Figure 3.1d and Figure B6). Figure 3.3 shows nanovalve function testing for MLD treated MCM-48-zeolite 5A calcined at 450°C after one, two, and three cycles of testing. The methane stored gradually decreases until stabilization at 55.8– 58.4% (40.7–42.6 V/V) of the maximum storage capacity of zeolite 5A, which was about 200% higher than storage capacity of the uncoated 5A beads at the same storage pressure, which suggested good stability and reversibility of our nanovalved adsorbents for CH<sub>4</sub> storage.

Ideally, all the adsorbed methane at the loading pressure would be maintained at the storage, however, not all the zeolite 5A beads are coated continuous. Some of the zeolite 5A beads have cracks or low quality coverage in the MCM-48 layer. For this reason, the above reported methane storage is lower than the maximum methane saturation capacity of the bare zeolite 5A beads. Therefore, to improve the performance, methods to continuously coat all the zeolite 5A beads uniformly without defects or an efficient method to screen for only the high quality beads must be investigated.

The methane stored in the nanovalve materials is also deliverable. By increasing the temperature of the sorbent system (Appendix B), the nanovalve layer can be reopened allowing the methane stored within the sample to be released.

Figure 3.4 shows a comparison of the above described nanovalve adsorbents with MOFs and COFs for methane storage. The nanovalve adsorbents prepared and tested as described have a methane storage capacity at 1bar 5-7 times higher than the methane storage capacity of other reported materials at 7-15bar.

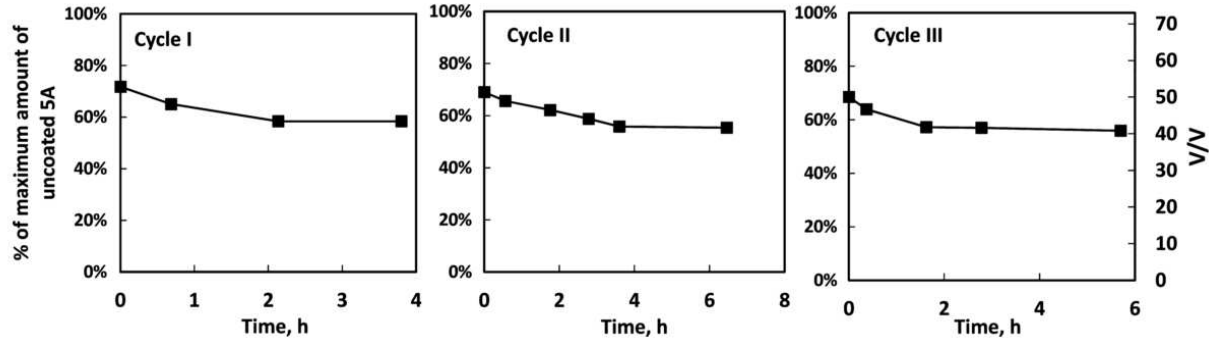


Figure 3.3. Three cycles of CH<sub>4</sub> storage test on MLD-MCM-48-5A adsorbent (loading pressure 50 bar, storage pressure 1 bar)<sup>36</sup>

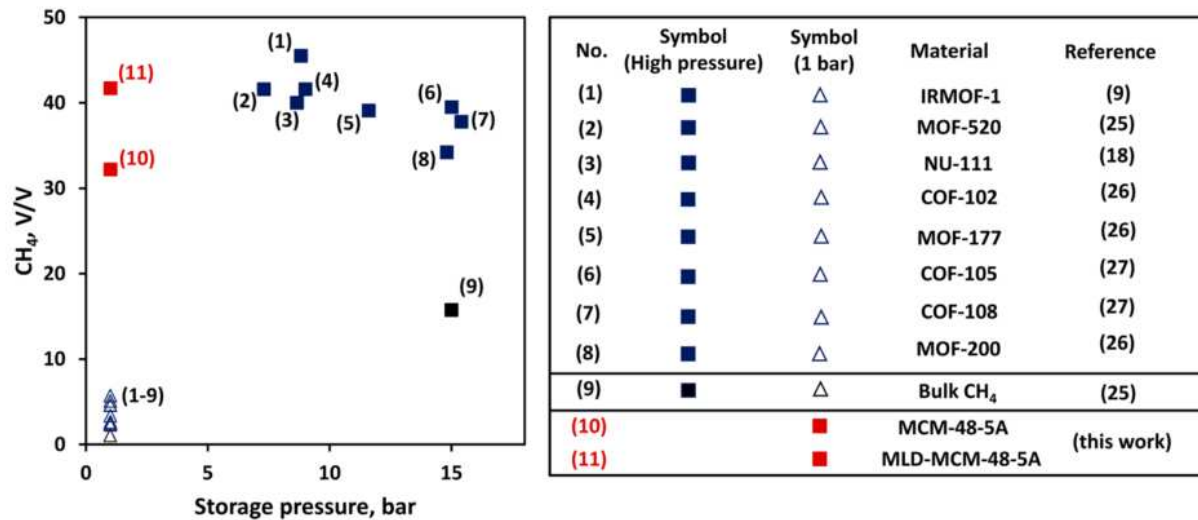


Figure 3.4. Comparison of nanovalve adsorbents with porous materials for CH<sub>4</sub> storage: CH<sub>4</sub> storage amount versus CH<sub>4</sub> storage pressure. Blue squares and triangles (1–8) represent porous materials from the literature;<sup>9,18,25–27</sup> bulk density of methane is represented by black square and triangle (9);<sup>25</sup> red squares (10–11) indicate nanovalve adsorbents from this study.<sup>36</sup>

The information presented in this Chapter serves as a proof-of-concept for the hypothesized nanovalve storage technique. As shown, coating a porous layer on an adsorbent pellet, can be loaded at high pressure, sealed, and then be stored at low pressure while maintaining a large percentage of the initially loaded methane. Although, as reported, the best nanovalve sample (MLD-MCM-48-5A) can hold only 40.7–42.6 V/V. However, this corresponds to almost 60% of the maximum methane saturation capacity of the coated adsorbent. Therefore, it is feasible by choosing a higher uptake adsorbent and improving the quality of the nanovalve layer that the ARPA-E target could potentially be reached at low storage pressure. As shown in Table B3, MOF-177,<sup>58</sup> COF-102,<sup>21</sup> and COF-105-Eth-trans,<sup>21</sup> loaded with methane at 250bar could meet the energy density targets set by ARPA-E (volumetric energy density >12.5 MJ/L, gravimetric energy density >0.5 g CH<sub>4</sub>/g sorbent).

## CHAPTER 4

### ZEOLITE ADSORBENT-MOF LAYERED NANOVALVES FOR CH<sub>4</sub> STORAGE

In this Chapter, the nanovalve concept outlined in the previous chapter is further investigated using MOFs as sealing layers.<sup>59</sup> As discussed previously, the integrity and properties of the nanovalving layer coated on the pelleted adsorbent is paramount. Using a well-defined and research MOF, HKUST-1, four isostructural materials were synthesized and used as nanovalving layers on zeolite 5A beads to isolate the impact of different coordinating metals on nanovalve adsorbent performance. These MOFs included HKUST-1, Al-MOF, Ga-MOF, and Co-MOF. Because the continuity and integrity of the nanovalve coating is important, one, two, and three layers of each of the four MOFs were coated on the zeolite 5A beads. The results to be discussed show that two layers of MOF display the best performance regardless of coordinating metal. The methane storage capacity followed the order: Al-MOF>Ga-MOF>Co-MOF>Cu-MOF. The best performing material, 2-layer Al-MOF, was able to store 33.6 (L STP methane/L nanovalve adsorbent) excess methane, corresponding to 46% of the methane saturation capacity of the zeolite 5A bead adsorbent at <1bar.

HKUST-1<sup>29</sup> has been the subject of various research studies including hydrogen storage<sup>60</sup>, carbon dioxide capture and separation<sup>31</sup>, encapsulation of ionic liquids<sup>61</sup>, and natural gas storage<sup>13</sup> among others. In particular, HKUST-1 has been chosen as a nanovalving layer because it has been shown to be a highly adsorptive material.<sup>35,62–64</sup> Therefore, it is likely that ethanol can be adsorbed into the nanovalving layer to more strongly seal in the adsorbent methane.

The synthesis of the four isostructural MOFs was carried out based on a recent report using aluminum and gallium as coordinating metals in the HKUST-1 structure.<sup>65</sup> Instead of using the, typically, moderate synthesis temperature (~120°C) and moderate synthesis times (12-18 hours)<sup>60</sup>, 180°C for 24 hours was used as reported for the Al- and Ga-MOF for all four of the MOFs.<sup>65</sup> In the next paragraphs the synthesis of Al-MOF- zeolite 5A beads nanovalves is described. The synthesis of the other three MOF nanovalves, and characterization methods are described in detailed in Appendix A.

Aluminum isopropoxide (0.5269g) was dissolved in 15 mL of DI water by sonication for 5 minutes followed by stirring at 50°C. 1,3,5-Benzenetricarboxylic acid (0.3993g) was dissolved in 15 mL of 50/50 ethanol/DI water by stirring. The two solutions were then mixed for ~5 minutes and transferred to an autoclave. Hydrothermal treatment was carried out at 180°C for 24 hours. The crystals were rinsed three times with 50/50 ethanol/DI water and collected by centrifugation. The resultant crystals were then dried at 80°C.

The Al-MOF layer was grown on zeolite 5A beads via secondary seeded approach. Typically, 5g of zeolite 5A beads were heated at 150°C for ~5 minutes. An Al-MOF solution was prepared by sonicating 0.2g Al-MOF crystals (prepared as described above) in 9.8g of DI water (~2wt% suspension). The hot zeolite 5A beads were poured directly in the ~2 wt% suspension and sonicated for 5 minutes. To enhance crystal attachment in the surface of the zeolite 5A beads, this procedure was repeated three times using the same crystal suspension. The “seeded zeolite 5A beads” were dried at 100°C overnight. For the Al-MOF layer(s) synthesis on 5A zeolite beads, aluminum isopropoxide (0.5269g) was dissolved in 15 mL of water by sonication for 5

minutes followed by stirring at 50°C. 1,3,5-Benzenetricarboxylic acid (0.3993g) was dissolved in 15 mL of 50/50 ethanol/DI water by stirring. The two solutions were mixed for 5 minutes and transferred to an autoclave containing the “seeded zeolite 5A beads”. After hydrothermal treatment at 180°C for 24 hours the sample was rinsed three times with DI water and dried overnight at 80°C. This procedure was repeated twice and three times to obtain 2 layer and 3 layer Al-MOF nanovalved adsorbent.

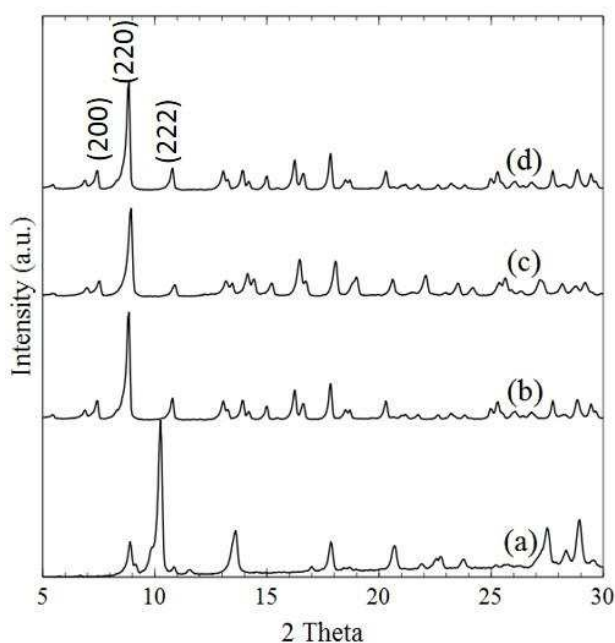


Figure 4.1. XRD patterns of the as-synthesized crystals (a) HKUST-1 (b) GaMOF (c) AlMOF and (d) CoMOF. Peak indexes are from Lin *et al*<sup>60, 59</sup>

After the four MOFs were synthesized as crystals, x-ray diffraction (Siemens Kristalloflex 810,  $\text{Cu}_{\text{K}\alpha}$  x-ray source, 0.154nm wavelength) was used to confirm that all four were isostructural. The XRD patterns for the four MOF materials are presented in Figure 4.1. The pattern for HKUST-1 matches the literature XRD patterns published previously.<sup>60</sup> The peaks for the Al-, Ga-, and Co-MOFs do not perfectly align with those

of HKUST-1, however, the arrangement and intensity of the peaks correspond with the HKUST-1 crystal structure. The shift of the peaks is due to the difference in the atomic size of the different coordinating metals incorporated into the framework (Co atomic radius = 0.125 nm; Cu atomic radius = 0.127 nm; Ga atomic radius=0.136 nm; Al atomic radius = 0.143 nm)<sup>66</sup>. The same shift of XRD peaks was observed for the Al- and Ga-MOF published previously.<sup>65</sup>

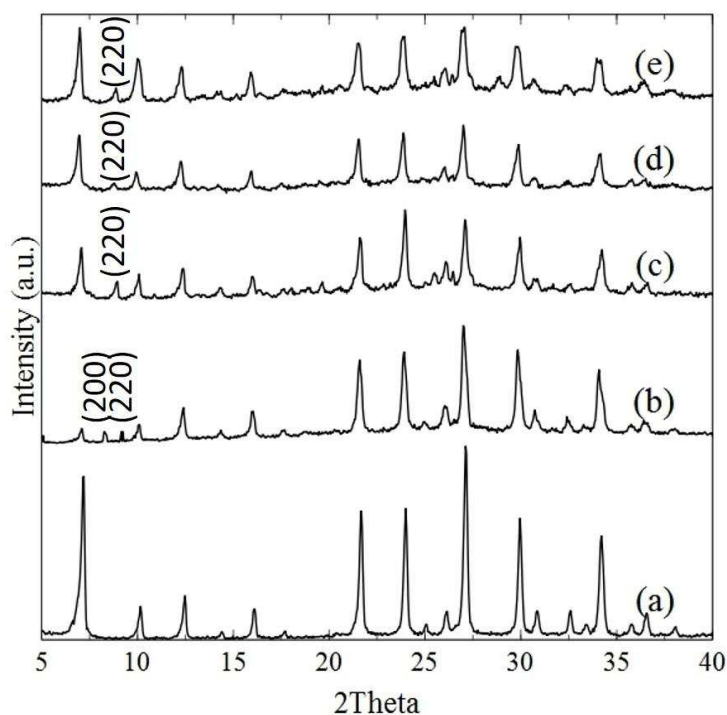


Figure 4.2. XRD for crushed (a) bare zeolite 5A beads and crushed 2-layer samples of (b) AlMOF (c) GaMOF (d) CoMOF and (e) HKUST-1 on zeolite 5A beads. MOF peaks are indexed from Lin et al<sup>60</sup>.<sup>59</sup>

To ensure the MOFs were being coated on the zeolite 5A beads and to better understand how the layers were being grown on the zeolite 5A beads, two-layer MOF-zeolite 5A nanovalves for each of the four MOFs were crushed and subjected to x-ray

diffraction. The patterns collected are presented in Figure 4.2. As seen, an extra peak around  $2\theta \sim 9^\circ$  is present in the MOF-zeolite 5A nanovalve patterns that is not in the bare zeolite 5A bead control pattern. By noting the peak plane indexes, HKUST-1, Ga-MOF, and Co-MOF grow on the zeolite 5A beads to preferentially expose the (220) while the Al-MOF grows to preferentially expose both the (200) and (220) plane.

The nanovalve performance of one, two, and three layer nanovalves for each of the four MOFs was tested using an in-house apparatus (Appendix A) that was designed and built specifically to test nanovalve performance. Using the procedure in Appendix, ~0.5g of MOF-zeolite 5A nanovalves were loaded into the apparatus and degassed at 180°C for two hours under vacuum. The nanovalve adsorbent was then loaded with methane at 50bar. Methane was redirected to a reference tank filled with ethanol. The ethanol saturated methane was flown over the nanovalve sample at 50bar for 2 hours to seal in the adsorbed methane. The pressure was reduced to ~1bar and the storage performance was recorded over a 48 hour period. Pressure versus time plots indicated that 48 hours was sufficient time for equilibrium to be reached as the pressure plateaus before 48 hours (Figure A2). After 48 hours, the nanovalve sample was heated to 100°C for 1 hour to release the methane maintained.

The performance results are shown in Figure 4.3. For each of the four MOFs, two-layers of MOF nanovalves perform better than the respective one and three layers of MOF nanovalves as well as the bare zeolite 5A bead control sample. To better understand why two-layer samples outperform one and three layer samples, representative SEM images of one, two, and three layer samples are presented in Figure A3. By inspecting the images, the quality and continuity of the two-layer samples

is superior to the one and three layer samples. Because layer quality is vital in the nanovalve process, the better performance of the two-layer samples is understandable.

In the case of the 1-layered materials, the lower performance can be associated to both the incomplete MOF coverage of the zeolite 5A beads and to the high methane capacity of the layer itself which can be displaced by ethanol (being of molecular size capable of fitting in the pores of the HKUST-1 framework). The ethanol and displaced methane are then exhausted when lowering the system pressure to ambient. The lowering in performance due to ethanol replacement is more evident in the 3-layered materials because of the increased amount of material making up the layer. Because the 2-layered materials performed better, the remainder of the discussion will focus only on these series of materials.

Figure 4.3 also shows a trend of performance according to coordinating in the order Al>Ga>Co>Cu. The methane storage of the two-layer Al-MOF, Ga-MOF, Co-MOF, and HKUST-1 were 33.6, 31.7, 17.5, and 15.5 respectively. Considering the maximum methane saturation capacity of the zeolite 5A beads was measured to be  $73 V/V^{36}$ , the best performing sample in this study, Al-MOF-zeolite 5A, was able to maintain ~46% of the maximum methane storage capacity at 1bar.

The performance data shows more variability in the HKUST-1 and Co-MOF samples than for the Al-MOF and Ga-MOF. SEM cross-section images of the four two-layer nanovalves (Figure 4.4) helps understand why there is a difference in variability. The Al-MOF and Ga-MOF grew on the surface of the zeolite 5A beads in a dense, intergrown layer. However, HKUST-1 and Co-MOF both grew on the surface of the zeolite 5A beads in a layer of needle or rod-like crystals. Figure 4.4 shows that there

are gaps in between the individual crystals of HKUST-1 and Co-MOF. These gaps are detrimental to the nanovalving process. The nanovalve function depends on sealing or closing the pores of the crystal structure of the material coated on the adsorbent. The gaps between the crystals give the methane adsorbed a path to diffuse out after the pressure is dropped in the testing procedure. The lower performance and higher variability for HKUST-1 and Co-MOF nanovalves illustrates the dependability of the nanovalve concept on integrity (well intergrown, low concentrate of defects, etc.) in the nanovalve layer.

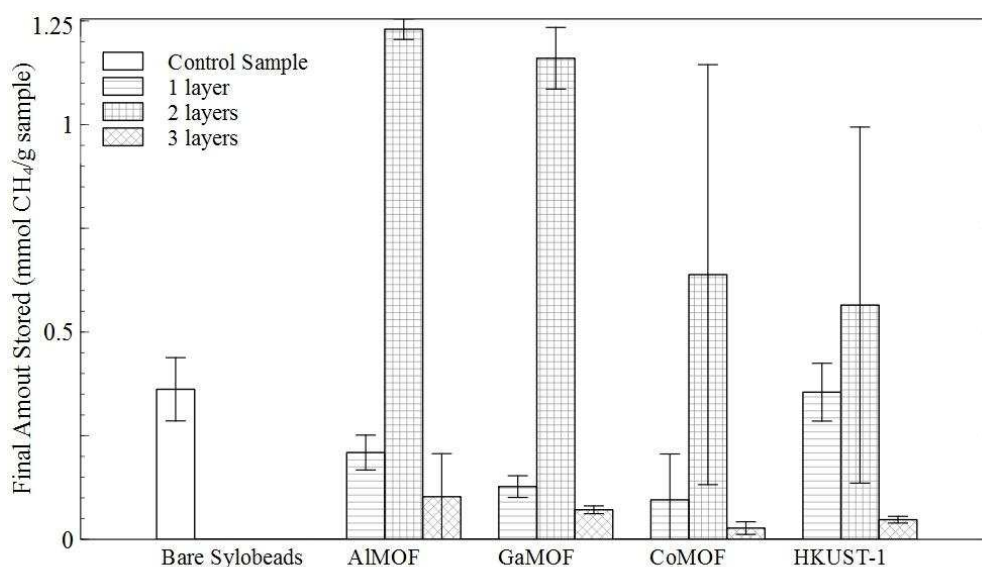


Figure 4.3. Nanovalve performance data obtained by in-house adsorption apparatus. The samples were degassed under vacuum for 2 hours and then loaded with methane to a pressure of 50 bar. The nanovalves were sealed by flow ethanol carried by methane at 50bar for 2 hours. After venting to ambient pressure, leak pressure was recorded for 48 hours before obtaining the final amount stored.<sup>59</sup>

The needle or rod-like crystal morphology of HKUST-1 shown in Figure 4.4 is atypical. The crystal morphology of HKUST-1 is known to be bipyramidal in shape.

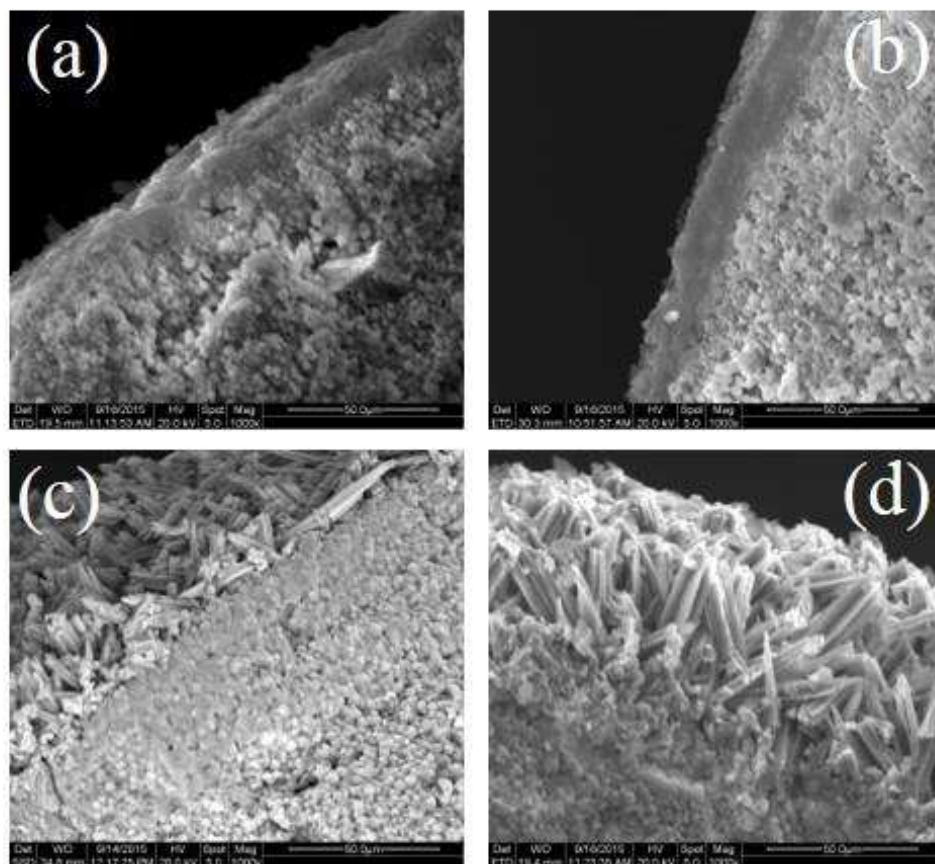


Figure 4.4. SEM images of 2-layers of (a) AlMOF (b) GaMOF (c) CoMOF and (d) HKUST-1 on zeolite 5A beads. The thicknesses for the MOF layers were Co-MOF  $\sim 7.5\mu\text{m}$ , Al-MOF  $\sim 10.5\mu\text{m}$ , Ga-MOF  $\sim 15.5\mu\text{m}$ , and HKUST-1  $\sim 27.5\mu\text{m}$ .<sup>59</sup>

This abnormality is attributed to the elevated synthesis conditions used to prepare the HKUST-1 in this study (180°C for 24 hours compared to the documented 110°C for 18 hours<sup>60</sup>). The synthesis conditions for all four MOFs were kept the same for this study to ensure that the only variable being test was coordinating metal. Because the HKUST-1 was atypical EDS chemical composition was carried out. It was confirmed that the copper to oxygen ratio was close to the ratio expected in the HKUST-1 framework (Table A3).

Though the focus of this study<sup>59</sup> was to establish a way to systematically test specific parameters of the nanovalving layer on the resulting nanovalve performance by way of testing several coordinating metals, the best performing nanovalve adsorbent, two-layer Al-MOF-zeolite 5A, performs similar to the nanovalve coating discussed in the previous proof of concept chapter. MCM-48-zeolite 5A after MLD modification provided methane storage of 42.6 V/V, however, MCM-48-zeolite 5A without MLD modification stored 32.2 V/V. The two-layer Al-MOF-zeolite 5A nanovalves discussed here was able to store 33.6 V/V. While the Al-MOF performs better than MCM-48 without MLD but worse than MCM-48 with MLD, there are several advantages of the nanovalves tested and discussed in this chapter over the MCM-48 nanovalves in the previous chapter. One advantage of the Al-MOF is less synthesis (24 hours/layer for the MOFs and 72 hours/layer for MCM-48). Another advantage of the MOF nanovalves, allow further conservation of time, is that the MOFs do not require a calcination step (about 12 hours for MCM-48) or post modification with MLD (although MLD could further enhance the performance of the MOF nanovalves discussed in this chapter). In addition to less synthesis time, the MOF nanovalves can be sealed using ethanol. Ethanol is cheaper

as compared to the DMB used in the MCM-48 nanovalve study. Though it has been reported that zeolite 5A exhibits an ethanol uptake of  $\sim 0.74$  mmol/g<sup>18</sup>, this is an order of magnitude less than the ethanol uptake reported for HKUST-1 of  $\sim 6.5$  mmol/g<sup>67</sup>.

In summary, a nanovalve adsorption method for high capacity storage of methane at low pressure is demonstrated employing metal organic frameworks as nanovalved layers. Four isostructural MOFs: Al-MOF, Ga-MOF, Co-MOF, and HKUST-1 were chosen as the nanovalve layers to coat zeolite 5A adsorbent beads. The MOF nanovalve adsorbents were loaded at 50bar with methane. The nanovalves were then closed with ethanol functioning as sealing molecule and lowered to ambient pressure. The performance of the MOF nanovalve adsorbents was evaluated by excess methane stored after opening the nanovalves via heating. Specifically, the impact of coordinating metal was studied in this chapter to better understand which factors in the nanovalving layer impacted CH<sub>4</sub> storage. The results demonstrate that the coordinating metal in the MOF structure does have a profound impact on the performance of the nanovalving method. The methane storage capacity followed the order: Al-MOF>Ga-MOF>Co-MOF>Cu-MOF. The best performing material, 2-layer Al-MOF, was able to store 33.6 V/V excess methane. Using ethanol, a cheap, renewable, and safe sealing agent, the 2-layer Al-MOF was able to hold  $\sim 46\%$  of the methane saturation capacity of the zeolite bead 5A adsorbent at <1bar.

## CHAPTER 5

### CONCLUSIONS AND RECCOMENDATIONS

The work that has been described in the previous chapters has shown the feasibility of the nanovalve natural gas (methane) storage technique. In both Chapter 3 and Chapter 4, the zeolite 5A adsorbent beads were able to maintain stored methane loaded at high pressure, but sealed and reduced to low pressure.

Chapter 3 demonstrates adding a layer of microporous material on an adsorbent pellet allows for the adsorbent to greatly increase the amount of methane stored at ambient pressure (200% more methane stored using nanovalving). MCM-48 coated zeolite 5A beads calcined at 450°C were able to maintain 44% (32 V/V) of the maximum methane capacity of the uncoated zeolite 5A beads (73 V/V). The work described in this chapter allows establishes the effectiveness of molecular layer deposition (MLD) to seal defects in the MCM-48 microporous layer and to decrease the characteristic pore size of the MCM-48 layer. After conducting three cycles of MLD on the MCM-48 coated zeolite 5A beads, the nanovalve material was able to maintain 55.8-58.4% (40.7-42.6 V/V) of the maximum capacity of the uncoated 5A beads. Though the zeolite 5A adsorbent beads used in this study does not allow for the ARPA-E target to be met even if 100% of the loaded methane was maintained, this study shows that even before trying lots of different materials for the nanovalve layer that more than half of the maximum capacity of the coated adsorbent can be maintained.

The work presented in Chapter 4 seeks to establish a method of deciding which parameters and properties of the nanovalve layer lead to increased performance in

methane storage. This study specifically uses the HKUST-1 structure to decide which coordinating metal among aluminum, gallium, copper, and cobalt is most advantageous for maintain a higher percentage of the maximum methane capacity of the zeolite 5A adsorbent beads. The HKUST-1 study also demonstrates that a cheaper, more environmentally friendly organic solvent (ethanol) can be used as a nanovalve sealing agent. The 2-layer MOF coated zeolite 5A beads out performed 1- and 3-layer MOF coated samples. Among the 2-layer coated materials, the Al-MOF performed the best—maintaining 46% (33.5 V/V) of the maximum methane capacity of the zeolite 5A beads. The effect of the coordinating metals tested was such that aluminum was the most advantageous, followed by gallium, followed by cobalt, followed by copper. The largest advantages of using the MOF layers over the MCM-48 layer are that the MOF layers require less synthesis time and a cheaper sealing agent (ethanol) still being able to almost achieve the same maintained capacity.

The major limitation for the work presented here is with the adsorbent being used. While zeolite 5A is among the highest methane adsorbing zeolites, the methane saturation capacity of zeolite 5A is well below the storage target set by ARPA-E. Zeolite 5A adsorbent beads, however, are useful in that they are easily accessible and provide a relatively cheap way to filter through nanovalve layers for highest percentage of methane maintained. Another limitation is that the materials tested at nanovalve layers present here is far from exhaustive. While a way to better decide which properties in the layer are desirable, there is a lot of room for expansion in improving the performance in the layer.

In the future, pursuing the fabrication of MOF adsorbing pellets is advisable. Many MOF materials have a methane saturation capacity above the ARPA-E target. These materials include HKUST-1, COF-103-eth-trans, and MOF-177 (mentioned in Chapter 2). Though the saturation pressure is higher than the 35bar target for these materials, the nanovalve concept illustrate here make the target achievable. Once MOF pellets are available and a method of fabrication is established, optimization of the nanovalving layer should be resumed. In resuming layer optimization, the best course of action would to be establish parameters and properties to examine (pore size, organic linker, coordinating metal, hydrophobicity, etc.). This method of optimization eliminates the need to test all materials as nanovalving layers without assurance of high performance. Instead, once a list of advantageous properties is established, a material containing the most of the desirable properties can be searched for or created.

In order to reach the methane saturation of MOF pellets, the loading pressure would have to be much higher (250-300bar) in future work than the 50bar used in the work presented here. Also, because the ARPA-E storage target is set at 35bar, investigating nanovalve storage pressures below 35bar but above ambient pressure could prove beneficial for adsorption/storage performance.

## REFERENCES

- (1) *The World Factbook* 2013-14. Washington, DC: Central Intelligence Agency, 2013. <https://www.cia.gov/library/publications/the-world-factbook/index.html>
- (2) Doman, L. U . S . remained world ' s largest producer of petroleum and natural gas hydrocarbons in 2014 <https://www.eia.gov/dnav/ng/hist/n9050us2a.htm>.
- (3) U.S. Energy Information Administration. Natural Gas <https://www.eia.gov/dnav/ng/hist/n9050us2a.htm>.
- (4) International Energy Agency, World Energy Outlook 2011: Are We Entering a Golden Age of Gas, [http:// www.worldenergyoutlook.org](http://www.worldenergyoutlook.org).
- (5) Wakamatsu, H.; Aruga, K. The Impact of the Shale Gas Revolution on the U.S. and Japanese Natural Gas Markets. *Energy Policy* 2013, 62, 1002–1009.
- (6) Services, A. E. Crude Oil and Natural Gas Move to Different Hemispheres <http://www.avalonenergy.us/blog/?p=376>.
- (7) Blazek, C. F.; Grimes, J.; Freeman, P.; Bailey, B. K.; Colucci, C. Fuel Composition Effects on Natural Gas Vehicle Emissions. In *207th ACS national meeting*; San Diego, CA, 1994.
- (8) Reilly, J.; Stone, P. H.; Forest, C. E.; Webster, M. D.; Jacoby, H. D.; Prinn, R. G. CLIMATE CHANGE: Uncertainty and Climate Change Assessments. *Science* (80- . ). 2001, 293 (5529), 430a – 433.
- (9) Remick, R.J. Tiller, A. J. Advanced Methods for Low-Pressure Storage of CNG. In *Proc. of Symposium on Nonpetroleum Vehicular Fuels V*; CNG Fuel: Arlington, 1985; pp 105–119.
- (10) Cracknell, R. F.; Gordon, P.; Gubbins, K. E. Influence of Pore Geometry on the Design of Microporous Materials for Methane Storage. *J. Phys. Chem.* 1993, 97 (2), 494–499.
- (11) Wegrzyn, J.; Gurevich, M. Adsorbent Storage of Natural Gas. *Appl. Energy* 1996, 55, 71–83.
- (12) Elliot, D. Topaloglu, T. The Development of New Adsorbent Materials for the Storage of Natural Gas on-Board Vehicles. In *Conf. Proc. of Gaseous Fuels for Transportation I*; Vancouver, 1986; pp 489–504.
- (13) Mason, J. A.; Veenstra, M.; Long, J. R. Evaluating Metal–organic Frameworks for Natural Gas Storage. *Chem. Sci.* 2014, 5, 32–51.
- (14) U.S Department of Energy. Alternative Fuels Data Center – Fuel Properties Comparison. *Energy Effic. Renew. Energy* 2014, 1–4.

- (15) Menon, V. C.; Komarneni, S. Porous Adsorbents for Vehicular Natural Gas Storage : A Review. *J. Porous Mater.* 1998, 5, 43–58.
- (16) Nam, G. M.; Jeong, B. M.; Kang, S. H.; Lee, B. K.; Choi, D. K. Equilibrium Isotherms of CH<sub>4</sub>, C<sub>2</sub>H<sub>4</sub>, C<sub>2</sub>H<sub>2</sub>, N<sub>2</sub>, and H<sub>2</sub> on Zeolite 5A Using a Static Volumetric Method. *J. Chem. Eng. Data* 2005, 50 (1), 72–76.
- (17) Saha, D.; Bao, Z.; Jia, F.; Deng, S. Adsorption of CO<sub>2</sub>, CH<sub>4</sub>, N<sub>2</sub>O, and N<sub>2</sub> on MOF-5, MOF-177, and Zeolite 5A. *Environ. Sci. Technol.* 2010, 44 (5), 1820–1826.
- (18) Lalik, E.; Mirek, R.; Rakoczy, J.; Groszek, A. Microcalorimetric Study of Sorption of Water and Ethanol in Zeolites 3A and 5A. *Catal. Today* 2006, 114 (2-3), 242–247.
- (19) Duren, T.; Sarkisov, L.; Yaghi, O. M.; Snurr, R. Q. Design of New Materials for Methane Storage. *Langmuir* 2004, 20 (7), 2683–2689.
- (20) Furukawa, H.; Ko, N.; Go, Y. B.; Aratani, N.; Choi, S. B.; Choi, E.; Yazaydin, A. O.; Snurr, R. Q.; O’Keeffe, M.; Kim, J.; Yaghi, O. M. Ultrahigh Porosity in Metal-Organic Frameworks. *Science* (80-. ). 2010, 329 (5990), 424–428.
- (21) Lan, J.; Coa, D.; Wang, W. High Uptakes of Methane in Li-Doped 3D Covalent Organic Frameworks. *Langmuir* 2010, 26 (1), 220–226.
- (22) Furukawa, H.; Yaghi, O. M. Storage of Hydrogen , Methane , and Carbon Dioxide in Highly Porous Covalent Organic Frameworks for Clean Energy Applications. *J. Am. Chem. Soc.* 2009, 131, 8875–8883.
- (23) Hu, J.; Zhao, J.; Yan, T. Methane Uptakes in Covalent Organic Frameworks with Double Halogen Substitution. *J. Phys. Chem. C* 2015, 119 (4), 2010–2014.
- (24) Zhou, Y.; Dai, M.; Zhou, L.; Sun, Y.; Su, W. Storage of Methane on Wet Activated Carbon: Influence of Pore Size Distribution. *Carbon N. Y.* 2004, 42 (8-9), 1855–1858.
- (25) Sun, Y.; Liu, C.; Su, W.; Zhou, Y.; Zhou, L. Principles of Methane Adsorption and Natural Gas Storage. *Adsorption* 2009, 15 (2), 133–137.
- (26) Yulong, W.; Fei, W.; Guohua, L.; Guoqing, N.; Mingde, Y. Methane Storage in Multi-Walled Carbon Nanotubes at the Quantity of 80 G. *Mater. Res. Bull.* 2008, 43 (6), 1431–1439.
- (27) Matranga, K. R.; Myers, A. L.; Glandt, E. D. Storage of Natural-Gas By Adsorption on Activated Carbon. *Chem. Eng. Sci.* 1992, 47 (7), 1569–1579.
- (28) Quinn, D. F.; MacDonald, J. a. Natural Gas Storage. *Carbon N. Y.* 1992, 30 (7), 1097–1103.

- (29) Chui, S. S.-Y.; Lo, S. M.-F.; Charmant, J. P. H.; Orpen, A. G.; Williams, I. D. R. EPORTS A Chemically Functionalizable Nanoporous Material. *Science* (80- ). 1999, 283, 1148–1150.
- (30) Borah, B.; Zhang, H.; Snurr, R. Q. Diffusion of Methane and Other Alkanes in Metal-Organic Frameworks for Natural Gas Storage. *Chem. Eng. Sci.* 2015, 124, 135–143.
- (31) Li, J.-R.; Ma, Y.; McCarthy, M. C.; Sculley, J.; Yu, J.; Jeong, H.-K.; Balbuena, P. B.; Zhou, H.-C. Carbon Dioxide Capture-Related Gas Adsorption and Separation in Metal-Organic Frameworks. *Coord. Chem. Rev.* 2011, 255, 1791–1823.
- (32) Sun, B.; Kayal, S.; Chakraborty, A. Study of HKUST (Copper Benzene-1,3,5-Tricarboxylate, Cu-BTC MOF)-1 Metal Organic Frameworks for CH<sub>4</sub> Adsorption: An Experimental Investigation with GCMC (Grand Canonical Monte-Carlo) Simulation. *Energy* 2014, 76, 419–427.
- (33) Gomez-Gualdrón, D. A.; Wilmer, C. E.; Farha, O. K.; Hupp, J. T.; Snurr, R. Q. Exploring the Limits of Methane Storage and Delivery in Nanoporous Materials. *J. Phys. Chem. C* 2014, 118 (13), 6941–6951.
- (34) Mendoza-Cortes, J. L.; Pascal, T. A.; Goddard, W. A. Design of Covalent Organic Frameworks for Methane Storage. *J. Phys. Chem. A* 2011, 115, 13852–13857.
- (35) Gándara, F.; Furukawa, H.; Lee, S.; Yaghi, O. M. High Methane Storage Capacity in Aluminum Metal – Organic Frameworks. 2014, 10–13.
- (36) Song, Z.; Nambo, A.; Tate, K. L.; Bao, A.; Zhu, M.; Jasinski, J. B.; Zhou, S. J.; Meyer, H. S.; Carreon, M. A.; Li, S.; Yu, M. Nanovalved Adsorbents for CH<sub>4</sub> Storage. *Nano Lett.* 2016, 16 (5), 3309–3313.
- (37) Fachini, A.; Vasconcelos, M. T. S. D. Effects of Zeolites on Cultures of Marine Micro-Algae: A Brief Review. *Environ. Sci. Pollut. Res.* 2006, 13 (6), 414–417.
- (38) Mentastý, L.; Faccio, R. J.; Zgrablich, G. High-Pressure Methane Adsorption in 5A Zeolite and the Nature of Gas-Solid Interactions. *Adsorpt. Sci. Technol.* 1991, 8, 105–113.
- (39) Rolniak, P.; Kobayashi, R. Adsorption of Methane and Several Mixtures of Methane and Carbon Dioxide at Elevated Pressures and near Ambient Temperatures on 5A and 13X Molecular Sieves by Tracer Perturbation Chromatography. *AiChE J.* 1980, 26 (4), 616–625.
- (40) Ding, T.-F.; Ozawa, S.; Yanazaki, T.; Watamuki, I.; Ogina, Y. A Generalized Treatment of Adsorption of Methane onto Various Zeolites. *Langmuir* 1988, 4 (11), 392–396.
- (41) Otto, K. Adsorption of Methane on Active Carbons and Zeolites. In *Proceedings*

*4th Int. Conf. Alternative Energy Sources*; Miami, 1981.

- (42) Wakasugi, Y.; Ozawa, S.; Ogino, Y. Physical Adsorption of Gases at High Pressure. *J. Colloid Interface Sci.* 1981, *79* (2), 399–409.
- (43) Zhang, S. Y.; Talu, O.; Hayhurst, D. T. High-Pressure Adsorption of Methane in Nax, Mgx, Cax, Srx, and Bax. *J. Phys. Chem.* 1991, *95* (4), 1722–1726.
- (44) Talu, O.; Zhang, S. Y.; Hayhurst, D. T. Effect of Cations on Methane Adsorption by Nay, Mgy, Cay, Sry, and Bay Zeolites. *J. Phys. Chem.* 1993, *97* (49), 12894–12898.
- (45) Quinn, D. F.; MacDonald, J. A.; Sosin, K. Microporous Carbons As Adsorbents for Methane Storage. *Prepr. Pap. - Am. Chem. Soc., Div. Fuel Chem.* 1994, *39*, 451–455.
- (46) Wegrzyn, J.; Wiesmann, H.; Lee, T. LOW PRESSURE STORAGE OF NATURAL GAS ON ACTIVATED CARBON Brookhaven of Applied Science National Laboratory , Upton , New York 11973-5000. *Post-Conference Proc. 1992 Annu. Automot. Technol. Dev.* 1992.
- (47) Barton, S. S.; Dacey, J. R.; Quinn, D. F. High Pressure Adsorption of Methane on Porous Carbons, Fundamentals of Adsorption. In *Proc. 1st Eng. Foundation Conference*; 1983.
- (48) Sosin, K. A.; Quinn, D. F. Using the High Pressure Methane Isotherm for Determination of Pore Size Distribution of Carbon Adsorbents. *J. Porous Mater.* 1995, *1* (1), 111–119.
- (49) Quinn, D. F.; Holland, J. A. Carbonaceous Material with High Micropore Volume and Low Micropore Volume and Process for Producing Same. U.S. Patent 5,091,820, 1991.
- (50) Jiang, S.; Zollweg, J. a; Gubbins, K. E. High-Pressure Adsorption of Methane and Ethane in Activated Carbon and Carbon Fibers. *J. Phys. Chem.* 1994, *98* (22), 5709–5713.
- (51) Peng, Y.; Krungleviciute, V.; Eryazici, I.; Hupp, J. T.; Farha, O. K.; Yildirim, T. Methane Storage in Metal – Organic Frameworks: Current Records, Surprise Findings, and Challenges. 2013.
- (52) Cote, A. P.; Benin, A. I.; Ockwig, N. W.; O’Keeffe, M.; Matzger, A. J.; Yaghi, O. M. Porous , Crystalline , Covalent Organic Frameworks. *Science* (80-. ). 2005, *310* (November), 1166–1171.
- (53) Goddard, W. A.; Mendoza-Cortes, J. L.; Han, S. S.; Furukawa, H.; Yaghi, O. M. Adsorption Mechanism and Uptake of Methane in Covalent Organic Frameworks: Theory and Experiment. *J. Phys. Chem. A* 2010, *114* (40), 10824–10833.

- (54) Li, B.; Wen, H. M.; Wang, H.; Wu, H.; Tyagi, M.; Yildirim, T.; Zhou, W.; Chen, B. A Porous Metal-Organic Framework with Dynamic Pyrimidine Groups Exhibiting Record High Methane Storage Working Capacity. *J. Am. Chem. Soc.* 2014, *136* (17), 6207–6210.
- (55) Song, Z.; Huang, Y.; Wang, L.; Li, S.; Yu, M. Composite 5A Zeolite with Ultrathin Porous TiO<sub>2</sub> Coating for Selective Gas Adsorption. *Chem. Commun. (Camb)*. 2015, *51* (2), 373–375.
- (56) Song, Z. N.; Huang, Y.; Xu, W. W.; Wang, L.; Bao, Y.; Li, S. G.; Yu, M. Continuously Adjustable, Molecular-Sieving “Gate” on 5A Zeolite for Distinguishing Small Organic Molecules by Size. *Sci. Reports* 2015, *5*, 13981.
- (57) Kresge, C. T.; Leonowicz, M. E.; Roth, W. J.; Vartuli, J. C.; Beck, J. S. Ordered Mesoporous Molecular Sieves Synthesized by a Liquid-Crystal Template Mechanism. *Nature* 1992, *359*, 710–712.
- (58) Chae, H. K.; Siberio-Perez, D. Y.; Kim, J.; Go, Y.; Eddaoudi, M.; Matzger, A. J.; O’Keeffe, M.; Yaghi, O. M. A Route to High Surface Area, Porosity and Inclusion of Large Molecules in Crystals. *Nature* 2004, *427*, 523–527.
- (59) Tate, K. L.; Li, S.; Yu, M.; Carreon, M. A. Zeolite Adsorbent-MOF Layered Nanovalves for CH<sub>4</sub> Storage. *Adsorption* Manuscript submitted for publication.
- (60) Lin, K.-S.; Adhikari, A. K.; Ku, C.-N.; Chiang, C.-L.; Kuo, H. Synthesis and Characterization of Porous HKUST-1 Metal Organic Frameworks for Hydrogen Storage. *Int. J. Hydrogen Energy* 2012, *37*, 13865–13871.
- (61) Luo, Q.; An, B.; Ji, M.; Park, S.-E.; Hao, C.; Li, Y. Metal–organic Frameworks HKUST-1 as Porous Matrix for Encapsulation of Basic Ionic Liquid Catalyst: Effect of Chemical Behaviour of Ionic Liquid in Solvent. *J. Porous Mater.* 2015, *22*, 247–259.
- (62) Min Wang, Q.; Shen, D.; Bülow, M.; Ling Lau, M.; Deng, S.; Fitch, F. R.; Lemcoff, N. O.; Semanscin, J. Metallo-Organic Molecular Sieve for Gas Separation and Purification. *Microporous Mesoporous Mater.* 2002, *55* (2), 217–230.
- (63) Castillo, J. M.; Vlugt, T. J. H.; Calero, S. Understanding Water Adsorption in Cu - BTC Metal - Organic Frameworks. *J. Phys. Chem. C* 2008, *112* (41), 15934–15939.
- (64) Küsgens, P.; Rose, M.; Senkovska, I.; Fröde, H.; Henschel, A.; Siegle, S.; Kaskel, S. Characterization of Metal-Organic Frameworks by Water Adsorption. *Microporous Mesoporous Mater.* 2009, *120* (3), 325–330.
- (65) Yang, L.; Ruess, G. L.; Carreon, M. A. Cu, Al and Ga Based Metal Organic Framework Catalysts for the Decarboxylation of Oleic Acid. *Catal. Sci. Technol.* 2015, *5*.

- (66) Callister, W.D., J.; Rethwisch, D. G. *Fundamentals of Materials Science and Engineering. An Integrated Approach*; John Wiley & Sons, 2012.
- (67) Rezk, A.; AL-Dadah, R.; Mahmoud, S.; Elsayed, A. Investigation of Ethanol/metal Organic Frameworks for Low Temperature Adsorption Cooling Applications. *Appl. Energy* 2013, 112, 1025–1031.

# APPENDIX A

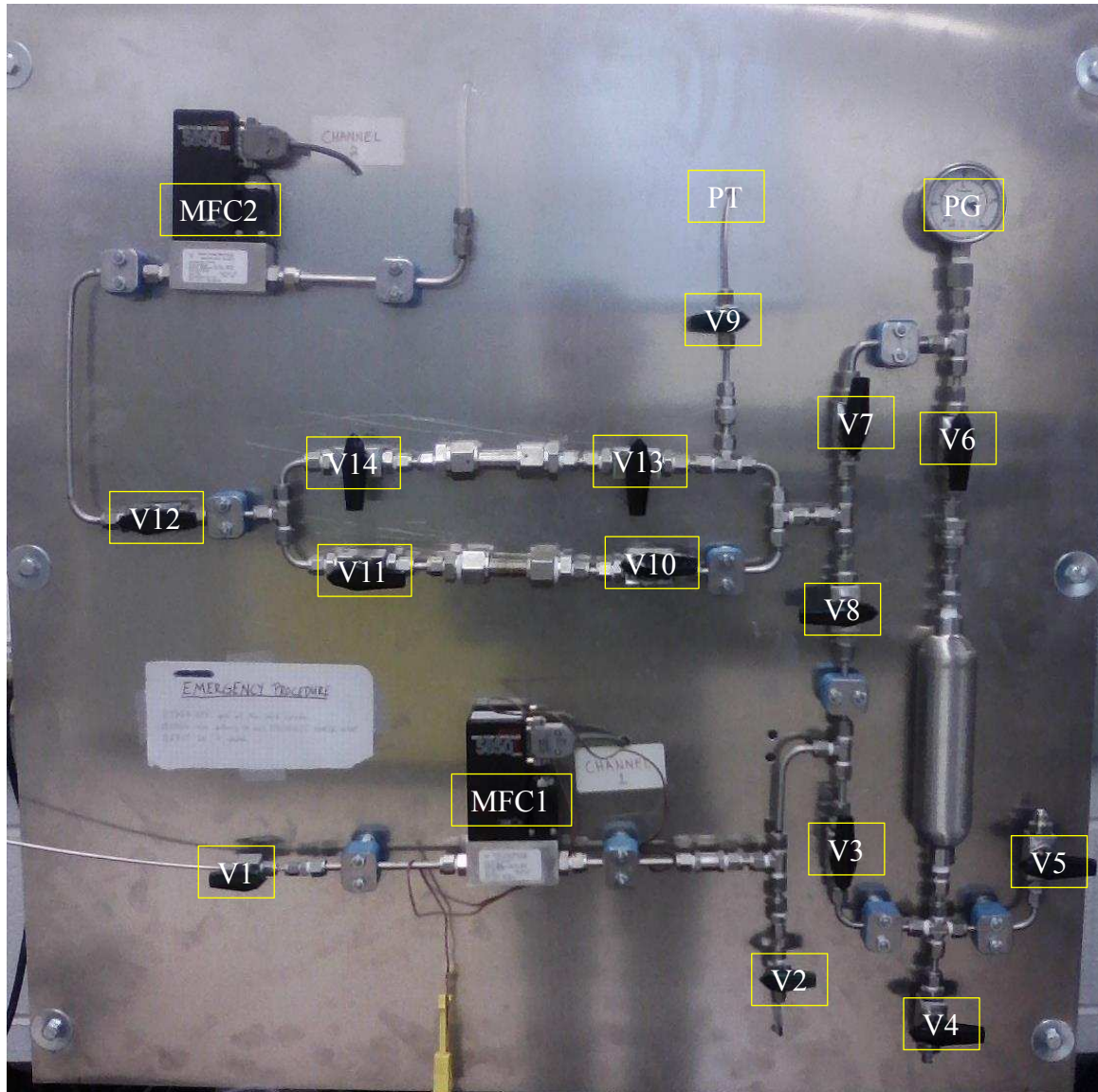


Figure A1. Nanovalve testing apparatus.

Table A1. Legend for nanovalue testing apparatus.

Designation	Description	Designation	Description
V1	Methane Inlet Valve	V10	Sample1 Inlet Valve
V2	Vacuum Valve	V11	Sample1 Exit Valve
V3	Gas to Sealant Valve	V12	Sample to Exhaust Valve
V4	Sealant Drain Valve	V13	Sample2 Inlet Valve
V5	Sealant Inlet Valve	V14	Sample2 Exit Valve
V6	Sealant to Sample Valve	MFC1	Inlet Mass Flow Controller
V7	Sample to PG Valve	MFC2	Exhaust Mass Flow Controller
V8	Gas to Sample Valve	PT	Pressure Transducer (0- 500psig)
V9	Pressure Transducer Valve	PG	Pressure Gauge (0-3000psig)

### Leak Testing Procedure

1. Vacuum entire volume of apparatus overnight (several hours). All valves are open EXCEPT Methane Inlet Valve (V1), Sealant Drain Valve (V4), and Sealant Inlet Valve (V5).

2. Measure approximately 0.5g of Nanovalve sample to be tested and record weight.
3. ALL valves are closed and the lower sample holder (Sample1) is removed. Place sample holder on scale and zero/tare. Plug one end of the sample holder with quartz wool. Pour the Nanovalve sample into the sample holder. Plug the other end with quartz wool. Weigh the sample holder and subtract Nanovalve sample weight. Record this weight as weight of quartz wool.
4. The thermocouple is wrapped around the sample holder followed by the heating tape. Aluminum foil is then wrapped around the thermocouple and heating tape followed by fabric insulation. This should be done such that the entire section between Sample1 Inlet Valve (V10) and Sample1 Exit Valve (V11) is covered.
5. All valves are closed EXCEPT Vacuum Valve (V2), Gas to Sample Valve (V8), Sample1 Inlet Valve (V10). This allows the sample to be under vacuum.
6. The sample is heated at 180°C under vacuum for 2 hours. When setting the temperature, the set point is ramped such that the temperature comes to 150°C first, then 170°C, and finally 180°C to avoid large overshoot.
7. The heating equipment (thermocouple, heating tape, aluminum foil, and fabric insulation) is removed. Wait 1 hour while the sample returns to room temperature (19°C in lab).
8. The Vacuum Valve (V2) is closed and the Methane Inlet Valve (V1) and Sample to PG Valve (V7) are opened. Set Inlet Mass Flow Controller (MFC1) to 100% open. Using the Pressure Gauge (PG), add methane until the pressure is

50barg. Monitor pressure using the Pressure Gauge (PG) to ensure the sample has reached equilibrium and the pressure is still 50barg (1 hour). Close ALL valves.

9. While waiting for the sample to come to equilibrium, the Sealant Inlet Valve (V5) is opened and ethanol is added with a pipette until the liquid is visible. The Sealant Inlet Valve (V5) is opened and closed several times to let air bubbles escape. Add more ethanol until the liquid is again visible. Close the Sealant Inlet Valve (V5).
10. After the 1 hour has passed, ALL valves are closed. The Vacuum Valve (V2), the Gas to Sample Valve (V8), the Sample to PG Valve (V7), and the Sealant to Sample Valve (V6) are opened. This section is vacuumed for 15 minutes to remove any lab air that may have entered while adding the sealant. ALL valves are closed.
11. The Methane Inlet Valve (V1), Gas to Sealant Valve (V3), and Sealant to Sample Valve (V6) are opened. The Inlet Mass Flow Controller (MFC1) is set to 100% open. Using the Pressure Gauge (PG), the pressure is set to 50barg. The Sample to PG Valve (V7) is opened. Using the Pressure Gauge (PG), the pressure is set again to 50barg. The Sample1 Exit Valve (V11) is opened. The pressure is set to 50barg. The Sample to Exhaust Valve (V12) is opened. The pressure is set to 50barg. The Inlet Mass Flow Controller (MFC1) and the Exhaust Mass Flow Controller (MFC2) are set to 10% open.
12. The sealant is allowed to flow over the sample at 50barg for 2 hours.

13. After the 2 hours have passed, the Methane Inlet valve is closed, the Inlet Mass Flow Controller (MFC1) is set to 0% open, and the Exhaust Mass Flow Controller (MFC2) is set to 100% open.
14. Once the Pressure Gauge (PG) reads the pressure is under 500psig, the Pressure Transducer Valve (V9) is opened. From here the Pressure Transducer (PT) is used to monitor when the system achieves atmospheric pressure (about 0.09 psig). Once the pressure is about 50psig, the Gas to Sample Valve (V8) and the Sample to PG Valve (V7) are closed. To monitor when the system achieves atmospheric pressure, the pressure is graphed by the OMEGA software. When the pressure graph is flat (not varying more than 0.05 psig), the system is said to be at atmospheric pressure. This takes about 30 minutes to achieve.
15. Once the system achieves atmospheric pressure, the OMEGA software is used to start plotting the pressure over time and recording the pressure over time. The Sample1 Exit Valve (V11) is closed. The OMEGA software reads and records the pressure 10 times every second. This rate is kept until the graph shows the pressure has passed the initial steep increase and has started the gradual increase. The rate at which the OMEGA software reads and records pressure is changed to once every 30s. The system is left in this state to record the leaking of the methane from the nanovalves for 48hours.
16. At the end of the 48hours, ALL valves are closed. The heating equipment is wrapped around the sample holder as before (see step 4).

17. The sample is heat at 100°C for 1 hour to force the methane to desorb from the sample. During this 1 hour, the Vacuum Valve (V2), Gas to Sample Valve (V8), and the Pressure Transducer Valve (V9) are opened.
18. After the 1 hour, the Gas to Sample Valve (V8) is closed and the Sample1 Inlet Valve (V10) is opened. Once the pressure levels off, 1 minute of pressure data is recorded using the OMEGA software at the 10 per 1s rating. The average these data points is used as the pressure for calculations.
19. ALL valves are closed. The Sealant Drain Valve (V4) and the Sealant Inlet Valve (V5) are opened. The ethanol is drained. The Sealant Drain Valve (V4) and the Sealant Inlet Valve (V5) are closed.
20. The sample holder is removed, the sample is removed, and the sample holder is reattached. All valves are opened EXCEPT the Sealant Drain Valve (V4) and the Sealant Inlet Valve (V5). The apparatus is under vacuum until the next day when the next test can be done.

#### Volume of Apparatus Procedure

1. All valves are closed. The lower sample holder (Sample1) is removed. A known amount of metal is loaded into the sample holder. The sample holder is returned to the apparatus.
2. The Vacuum Valve (V2), Gas to Sample Valve (V8), Pressure Transducer Valve (V9), and Sample1 Inlet Valve (V10) are opened.

3. Once the lowest vacuum is achieved, the Vacuum Valve (V2) is closed and the Methane Inlet Valve (V1) is opened. The Inlet Mass Flow Controller (MFC1) is set to 100% open. Helium is flown into the apparatus until an approximate set pressure is met.
4. The Methane Inlet Valve (V1) and the Gas to Sample Valve (V8) are closed. The Inlet Mass Flow Controller (MFC1) is turned off.
5. Once the pressure becomes steady, the OMEGA software is used to record the pressure at 10 per 1s rate for 2 minutes. The average of these is used as the pressure (see  $P_1$  below).
6. The Sample1 Inlet Valve (V10) is closed and the Vacuum Valve (V2) and the Gas to Sample Valve (V8) are opened.
7. Once the lowest vacuum is achieved for 2 minutes, the Vacuum Valve (V2) and the Gas to Sample Valve (V8) are closed. The Sample1 Inlet Valve (V10) is opened.
8. Once the pressure becomes steady, the OMEGA software is used to record the pressure at 10 per 1s rate for 2 minutes. The average of these is used as the pressure (see  $P_2$  below).
9. All valves are closed. The lower sample holder (Sample1) is removed. The metal is taken out of the sample holder. The sample holder is returned to the apparatus.

10. The Vacuum Valve (V2), Gas to Sample Valve (V8), Pressure Transducer Valve (V9), and Sample1 Inlet Valve (V10) are opened.
11. Once the lowest vacuum is achieved, the Vacuum Valve (V2) is closed and the Methane Inlet Valve (V1) is opened. The Inlet Mass Flow Controller (MFC1) is set to 100% open. Helium is flown into the apparatus until an approximate set pressure is met.
12. The Methane Inlet Valve (V1) and the Gas to Sample Valve (V8) are closed. The Inlet Mass Flow Controller (MFC1) is turned off.
13. Once the pressure becomes steady, the OMEGA software is used to record the pressure at 10 per 1s rate for 2 minutes. The average of these is used as the pressure (see P<sub>3</sub> below).
14. The Sample1 Inlet Valve (V10) is closed and the Vacuum Valve (V2) and the Gas to Sample Valve (V8) are opened.
15. Once the lowest vacuum is achieved for 2 minutes, the Vacuum Valve (V2) and the Gas to Sample Valve (V8) are closed. The Sample1 Inlet Valve (V10) is opened.
16. Once the pressure becomes steady, the OMEGA software is used to record the pressure at 10 per 1s rate for 2 minutes. The average of these is used as the pressure (see P<sub>4</sub> below).
17. Steps 10-16 from Volume of Apparatus Procedure are repeated.

## Solid Volume Procedure

1. After step 20 from Leak Testing Procedure, all valves are closed. The Vacuum Valve (V2), Gas to Sample Valve (V8), Pressure Transducer Valve (V9), and Sample1 Inlet Valve (V10) are opened.
2. Once the lowest vacuum is achieved, the Vacuum Valve (V2) is closed and the Methane Inlet Valve (V1) is opened. The Inlet Mass Flow Controller (MFC1) is set to 100% open. Helium is flown into the apparatus until an approximate set pressure is met.
3. The Methane Inlet Valve (V1) and the Gas to Sample Valve (V8) are closed. The Inlet Mass Flow Controller (MFC1) is turned off.
4. Once the pressure becomes steady, the OMEGA software is used to record the pressure at 10 per 1s rate for 2 minutes. The average of these is used as the pressure (see  $P_1$  below).
5. The Sample1 Inlet Valve (V10) is closed and the Vacuum Valve (V2) and the Gas to Sample Valve (V8) are opened.
6. Once the lowest vacuum is achieved for 2 minutes, the Vacuum Valve (V2) and the Gas to Sample Valve (V8) are closed. The Sample1 Inlet Valve (V10) is opened.
7. Once the pressure becomes steady, the OMEGA software is used to record the pressure at 10 per 1s rate for 2 minutes. The average of these is used as the pressure (see  $P_2$  below).

8. Steps 1-7 from Solid Volume Procedure are repeated.

## ANALYSIS

### Calculating the volume of the apparatus

The volume of the apparatus that is used during leak testing and the volume of the sample holder section is calculated using the following equations.

$$V_1 = \frac{\frac{\alpha b}{P_2}}{\left(\frac{\alpha}{P_2} - \frac{\beta}{P_4}\right)}$$

$$V_2 = \frac{\beta V_1}{P_4}$$

$$V_{TOT} = V_1 + V_2$$

$$V_{QW} = \frac{m_{QW}}{\rho_{QW}}$$

where

$V_1$ =volume of sample holder section (enclosed between valves V10 and V11), mL

$V_2$ =volume enclosed between valves V7, V8, V10, V13, and PT, mL

$V_{TOT}$ =total volume of apparatus occupied during leak testing, mL

$V_{QW}$ =volume of quartz wool, mL

$m_{QW}$ =mass of quartz wool, g

$\rho_{QW}$ =density of quartz wool, g/mL

b=known volume of metal, 0.71mL

P<sub>1</sub>=absolute pressure loaded to V<sub>1</sub> with metal, torr

P<sub>2</sub>=absolute pressure resulting from release to V<sub>2</sub> with metal, torr

P<sub>3</sub>=absolute pressure loaded to V<sub>1</sub> without metal, torr

P<sub>4</sub>= absolute pressure resulting from release to V<sub>2</sub> without metal, torr

α=P<sub>1</sub>-P<sub>2</sub>, torr

β=P<sub>3</sub>-P<sub>4</sub>, torr

#### Calculating volume of solid not able to be occupied by bulk gas

The volume not able to be occupied is found using Boyle's Law.

$$V_{solid} = \frac{P_1 V_1 - P_2 V_{TOT}}{\alpha}$$

where

V<sub>solid</sub>= volume of the sample not able to be occupied by bulk gas, mL

P<sub>1</sub>= absolute pressure loaded to V<sub>1</sub> with sample, torr

P<sub>2</sub>= absolute pressure loaded to V<sub>1</sub> with sample, torr

V<sub>1</sub>, V<sub>TOT</sub>, and α=as previously defined

#### Amount of methane leaked calculation

The total amount of methane leaked is found by using the ideal gas law and the pressure over time data collected.

$$n_L = \frac{P_{FLP}(V_{TOT} - V_{solid} - V_{QW})}{RT_{RM}}$$

where

$n_L$ =total number of moles of methane leaked, mol

$P_{FLP}$ =final leak pressure (or storage pressure), psig

$V_{TOT}$ =total volume occupied while measuring leaking, L

$V_{solid}$ =volume of the sample not able to be occupied by bulk gas, L

$V_{QW}$ =volume of quartz wool, mL

$T_{RM}$ =room temperature, 19°C

$R$ =ideal gas constant, 1.206 psig L mol<sup>-1</sup> K<sup>-1</sup>

#### Amount of bulk gas in sample holder at storage pressure calculation

The bulk gas in the sample holder at storage pressure is found by using the ideal gas law and the final leak pressure (or storage pressure).

$$n_{bulk} = \frac{P_{FLP}(V_1 - V_{solid} - V_{QW})}{RT_{RM}}$$

where

$n_{bulk}$ =moles of bulk methane in sample holder volume (between V10 and V11), mol

$V_1$ =volume between V10 and V11, L

$P_{FLP}$ =as previously defined, psia

$R$ ,  $T_{RM}$ ,  $V_{solid}$ ,  $V_{QW}$ =as previously defined with previous units

## Final amount of methane stored in nanovalve calculation

This calculation allows the amount of methane that was stored and NOT leaked.

$$n_{stored} = \frac{P_{DP}(V_1 - V_{solid} - V_{QW})}{RT_{DT}} + \frac{P_{DP}V_2}{RT_{RM}} - n_{bulk}$$

where

$n_{stored}$ =amount of methane stored, mol

$P_{DP}$ =desorption pressure, psia

$T_{DT}$ =desorption temperature, 100°C

$V_{TOT}$ ,  $T_{RM}$ ,  $V_{solid}$ ,  $R$ ,  $n_{bulk}$ ,  $V_{QW}$  =as previously defined or calculated

### *Materials for MOF Nanovalve Synthesis and Testing*

For the synthesis of MOF crystals and layers the following chemicals were employed. Copper (II) nitrate hemi(pentahydrate) (98%, Alfa Aesar), cobalt (II) nitrate hexahydrate ( $\geq 98\%$ , Sigma Aldrich), gallium (III) nitrate hydrate (99.9%, Sigma Aldrich), and aluminum isopropoxide (99.9, Sigma Aldrich) were used as the coordinating metal sources. 1,3,5-benzenetricarboxylic acid (98%, Alfa Aesar) was used as the organic linker, and ethanol (200 proof, Decon Labs, Inc.) and DI water were used as solvents. 5A zeolite beads (2.5 mm diameter from W.R. Grace & Co) were used as adsorbents, and served as substrates on which the MOF layers were grown.

### *Ga-MOF Nanovalved Adsorbent Synthesis*

*Crystal Synthesis.* Gallium (III) nitrate hydrate (0.6593g) was dissolved in 15 mL of DI water by stirring. 1,3,5-Benzenetricarboxylic acid (0.3993g) was dissolved in 15 mL of

50/50 ethanol/DI water by stirring. The two solutions were then mixed for 5 minutes and transferred to an autoclave. Hydrothermal treatment was carried out at 180°C for 24 hours. The crystals were rinsed three times with 50/50 ethanol/DI water and collected by centrifugation. The resultant crystals were then dried at 80°C.

*Ga-MOF Nanovalved Adsorbent Synthesis by Secondary Seeded Growth.* The Ga-MOF layer was grown on zeolite 5A beads via secondary seeded approach. Typically, 5g of zeolite 5A beads were heated at 150°C for ~5 minutes. A Ga-MOF solution was prepared by sonicating 0.2g Ga-MOF crystals (prepared as described in 2.3.1) in 9.8g of DI water (~2wt% suspension). The hot zeolite 5A beads were poured directly in the ~2 wt% suspension and sonicated for 5 minutes. To enhance crystal attachment in the surface of the zeolite 5A beads, this procedure was repeated three times using the same crystal suspension. The “seeded zeolite 5A beads” were dried at 100°C overnight. For the Ga-MOF layer(s) synthesis on 5A zeolite beads, gallium (III) nitrate hydrate (0.6593g) was dissolved in 15 mL of water by stirring. 1,3,5-Benzenetricarboxylic acid (0.3993g) was dissolved in 15 mL of 50/50 ethanol/water by stirring. The two solutions were mixed for 5 minutes and transferred to an autoclave containing the “seeded zeolite 5A beads”. After hydrothermal treatment at 180°C for 24 hours the sample was rinsed three times with DI water and dried overnight at 80°C. This procedure was repeated twice and three times to obtain 2 layer and 3 layer Ga-MOF nanovalved adsorbent.

#### *Co-MOF Nanovalved Adsorbent Synthesis*

*Crystal Synthesis.* Cobalt (II) nitrate hexahydrate (0.751g) was dissolved in 15 mL of DI water by stirring. 1,3,5-Benzenetricarboxylic acid (0.4g) was dissolved in 15 mL of 50/50 ethanol/DI water by stirring. The two solutions were then mixed for 5 minutes and

transferred to an autoclave. Hydrothermal treatment was carried out at 180°C for 24 hours. The crystals were rinsed three times with 50/50 ethanol/DI water and collected by centrifugation. The resultant crystals were then dried at 80°C.

#### *Co-MOF Nanovalved Adsorbent Synthesis by Secondary Seeded Growth.*

The Co-MOF layer was grown on zeolite 5A beads via secondary seeded approach. Typically, 5g of zeolite 5A beads were heated at 150°C for ~5 minutes. A Co-MOF solution was prepared by sonicating 0.2g Co-MOF crystals (prepared as described in 2.4.1) in 9.8g of DI water (~2wt% suspension). The hot zeolite 5A beads were poured directly in the ~2 wt% suspension and sonicated for 5 minutes. To enhance crystal attachment in the surface of the zeolite 5A beads, this procedure was repeated three times using the same crystal suspension. The “seeded zeolite 5A beads” were dried at 100°C overnight.

For the Co-MOF layer(s) synthesis on 5A zeolite beads, Cobalt (II) nitrate hexahydrate (0.751g) was dissolved in 15 mL of water by stirring. 1,3,5-Benzenetricarboxylic acid (0.4g) was dissolved in 15 mL of 50/50 ethanol/water by stirring. The two solutions were mixed for 5 minutes and transferred to an autoclave containing the “seeded zeolite 5A beads”. After hydrothermal treatment at 180°C for 24 hours the sample was rinsed three times with DI water and dried overnight at 80°C. This procedure was repeated twice and three times to obtain 2 layer and 3 layer Co-MOF nanovalved adsorbent.

#### *HKUST-1 Nanovalved Adsorbent Synthesis*

*Crystal Synthesis.* Copper (II) nitrate hemi(pentahydrate) (0.6g) was dissolved in 15 mL of DI water by stirring. 1,3,5-Benzenetricarboxylic acid (0.4g) was dissolved in 15 mL

of 50/50 ethanol/DI water by stirring. The two solutions were then mixed for 5 minutes and transferred to an autoclave. Hydrothermal treatment was carried out at 180°C for 24 hours. The crystals were rinsed three times with 50/50 ethanol/DI water and collected by centrifugation. The resultant crystals were then dried at 80°C.

*Secondary Seeded Growth.* The HKUST-1 layer was grown on zeolite 5A beads via secondary seeded approach. Typically, 5g of zeolite 5A beads were heated at 150°C for ~5 minutes. A HKUST-1 solution was prepared by sonicating 0.2g HKUST-1 crystals (prepared as described in 2.5.1) in 9.8g of DI water (~2wt% suspension). The hot zeolite 5A beads were poured directly in the ~2 wt% suspension and sonicated for 5 minutes. To enhance crystal attachment in the surface of the zeolite 5A beads, this procedure was repeated three times using the same crystal suspension. The “seeded zeolite 5A beads” were dried at 100°C overnight.

For the HKUST-1 layer(s) synthesis on 5A zeolite beads, Copper (II) nitrate hemi(pentahydrate) (0.6g) was dissolved in 15 mL of water by stirring. 1,3,5-Benzenetricarboxylic acid (0.4g) was dissolved in 15 mL of 50/50 ethanol/DI water by stirring. The two solutions were mixed for 5 minutes and transferred to an autoclave containing the “seeded zeolite 5A beads”. After hydrothermal treatment at 180°C for 24 hours the sample was rinsed three times with DI water and dried overnight at 80°C. This procedure was repeated twice and three times to obtain 2 layer and 3 layer HKUST-1-MOF nanovalved adsorbent.

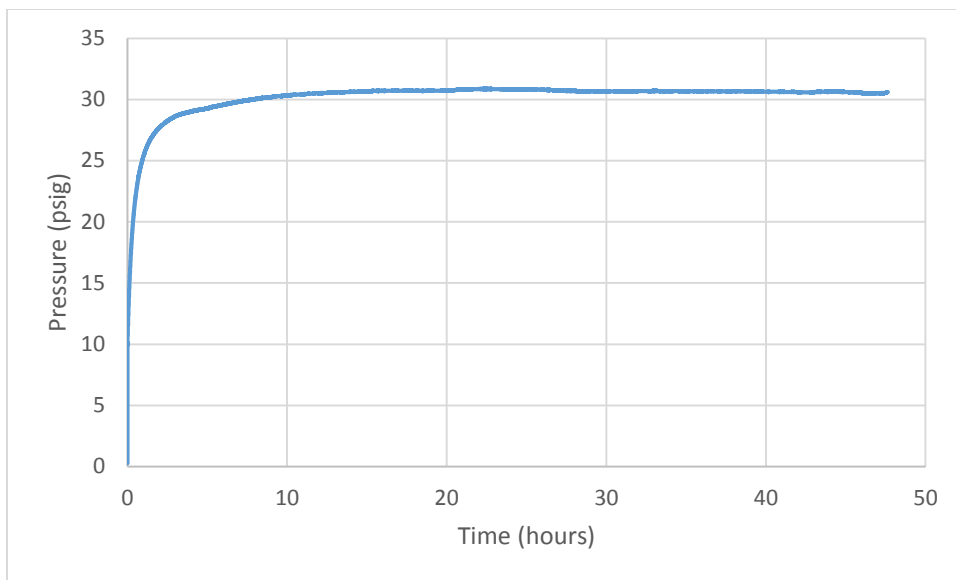


Figure A2. Storage pressure data for 1-layer GaMOF depicting stabilization well within 48hours.

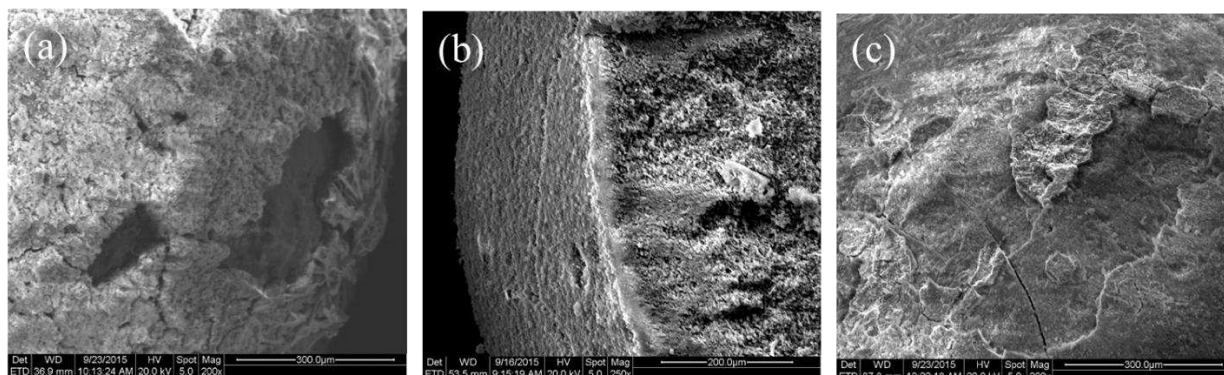


Figure A3. SEM of (a) 1-layer AIMOF, (b) 2-layer AIMOF, and (c) 3-layer AIMOF.

Table A2. BET surface area of the control and the four 2-layer nanovalve samples.

	BET Surface Area (m <sup>2</sup> /g)
Pure Sylobeads	549.0745
AlMOF_2L_B1_1C	546.9493
GaMOF_2L_B1_1C	507.6579
CoMOF_2L_B1_1C	445.9839
HKUST1_2L_B1_1C	549.8273

Table A3. EDX of HKUST-1 as-synthesized crystals.

Copper at%	Oxygen at%	O:Cu ratio
22.8	77.2	3.39
22.88	77.12	3.37
22.45	77.55	3.45
22.41	77.59	3.46
22.66	77.34	3.41
24.56	75.44	3.07
22.25	77.75	3.49
average over sample		
22.86	77.14	3.37

## APPENDIX B

Nano-valved adsorbent synthesis. MCM-48 solution was prepared by dissolving sodium hydroxide (98%, Sigma-Aldrich) and CTAB (cetyltrimethylammonium bromide) in deionized water at 40°C. The mixture was stirred for 30 minutes before adding TEOS (tetraethylorthosilicate). The molar composition of the solution was 1.0 TEOS: 0.48 CTAB: 0.46 NaOH: 56.0 H<sub>2</sub>O. The solution was stirred for another 60 minutes and then it was transferred to autoclave, in which the 5A zeolite beads (2.5 mm diameter from W.R.Grace & Co) were placed. The MCM-48 solution and the 5A zeolite beads were hydrothermally treated at 100°C for 72 h. Then, the coated beads were removed from the autoclave, washed gently with water, and dried at 120°C overnight. The template (CTAB) was removed by calcination in air in the 350-450 °C range for 4 h with a heating and cooling rate of 1°C/min.

Gas sorption measurement. Ultra-high purity CH<sub>4</sub> (99.999%), and He (99.999%) were purchased from Airgas. Gas adsorption isotherms were measured by a volumetric method using a home-built adsorption system. Sorbent was firstly outgassed at 200°C for 2 h. Helium was then used to calibrate the volume of adsorption cell with sorbent at 20°C. After vacuum to remove residue gasses in the adsorption system, CH<sub>4</sub> was introduced at 20°C. The pressure change was collected in real time using a Swagelok E model transducer (0.0-100.0 psia) for low pressure, an ASHCROFT (0-200 bar) transducer for high pressure, and LabVIEW 2012 software.

Nano-valve functioning test. In a typical nano-valve functioning test (Figure B3), approximately 0.5g of adsorbent is added to the adsorption tank. A vacuum pump is used to evacuate the sample at 200°C and reference lines before testing. Then, CH<sub>4</sub> is

introduced to the system at 50 bar and allowed enough time to reach equilibrium. When CH<sub>4</sub> adsorption reaches equilibrium at 50 bar, we then adjust the TESCO back pressure regulator (R1) and BROOKS 5850 E series mass flow controllers (MFC-1, MFC-2) to have CH<sub>4</sub> continuously introduced to the system by closing V3, opening the valves V2, V8, V7 and V4 to maintain the whole system pressure at about 50 bar. Next, sealing molecule (2,2-DMB) vapor, in the reference tank, will be blown into the adsorption tank by a slow CH<sub>4</sub> flow. The sealing molecule vapor is used to seal the porous coating layer on the adsorbents. After 1 h, the valve V2 is closed to stop feeding the CH<sub>4</sub>, while maintaining the valve V1, MFC-2 open and adjust the R1 to release the system pressure gradually from 50 bar to 1 bar within 1 h. After reaching ~1 bar, the storage system is closed (valves V1, V3, and V5 were closed) and the pressure change is monitored to calculate CH<sub>4</sub> leakage rate. After storage test, the sample cell is heated to 150°C to desorb the CH<sub>4</sub> sealed inside the coated adsorbents. The amount of CH<sub>4</sub> stored is calculated based on the system volume, pressure, and temperature.

Before we conducted QC testing for sorbents with coating, we examined the accuracy of calculating adsorbed CH<sub>4</sub> amount in sorbents by collecting CH<sub>4</sub> in gas phase by heating sorbents to 150-200°C. Specifically, we pressurized adsorption cell to ~2 bar and allowed CH<sub>4</sub> adsorption to reach steady state. Once it reached steady state, the adsorbed amount in sorbents will be known from the adsorption isotherm. Then, the adsorption cell will be heated to a desired temperature between 150 and 200 °C to desorb CH<sub>4</sub> to the gas phase. By comparing CH<sub>4</sub> in the gas phase before and after heating, adsorbed amount of CH<sub>4</sub> is calculated. From our experiments for 5 sorbents,

we found this method gave consistent adsorbed amounts with adsorption isotherm, and variation was within 3%. Therefore, our QC evaluation method is highly reliable.

Through these studies screened by low pressure QC test, the sample showed the highest amount of CH<sub>4</sub> stored will be selected for high pressure QC testing.

Molecular layer deposition on MCM-48-5A adsorbent. The MLD coatings were prepared by using trimethyl aluminum (TMA) (Al(CH<sub>3</sub>)<sub>3</sub>; 97%, Sigma Aldrich) and ethylene glycol (HO(CH<sub>2</sub>)<sub>2</sub>OH; 99%, Alfa Aesar) as precursors. Each MLD cycle started with 240 s vacuum. TMA was fed into the reactor until a pressure of 300 mTorr and then settled for 120 s; 240 s vacuum was followed to evacuate extra unreacted TMA. Ultrahigh purity N<sub>2</sub> (Airgas) was used as the purge gas at 20 sccm for 30 second. Then 240 s vacuum was applied to evacuate N<sub>2</sub>. Ethylene glycol (EG) was then introduced into the reactor until a pressure of 50 mTorr and settled for 120 s; then the above evacuation and purge operation were repeated for EG dosing. This whole process finishes one MLD cycle. MLD reactions were conducted at 100 °C. After 3 cycles of MLD modification, the coated samples were heated in air from room temperature to 250°C at a rate of 1°C/min, kept at 250°C for 4 h, and then cooled to room temperature at the same rate.

#### Characterization

SEM. SEM images were collected on a Nova NanoSEM 600 FEI with an acceleration voltage of 10 kV. EDX was carried out to determine the composition of selected samples.

High resolution transmission electron microscopy (HRTEM). FEI Tecnai F20 transmission electron microscope operated at 200 KV was used to analyze the pore

size of the MCM-48-5A and MLD-MCM-48-5A adsorbents. The samples were dispersed on lacey carbon films supported on 300 mesh TEM copper grids and Z-contrast scanning TEM (STEM) images were collected at spatial resolution of ~ 0.2 nm using nanoprobe and Fischione Model 3000 High Angle Annular Dark Field (HAADF) detector. ImageJ, freely available software, was used to analyze STEM images and measure pores size distributions.

BET. N<sub>2</sub> BET surface areas were collected in a Micromeritics Tristar-3000 porosimeter at 77 K using liquid nitrogen as coolant. Before measurements, the samples were degassed at 300 °C for 6 h.

Hg porosimetry. Hg measurements were collected in a Autopore IV porosimeter. The volume of mercury in the penetrometer's stem was measured by determining the penetrometer's electrical capacitance. Autopore IV software was used to convert this electrical capacitance into data points showing the volume of mercury penetrating the pores of the sample.

Estimation of the maximum holding pressure of nanopores filled with adsorbates

We used Young-Laplace equation to estimate to the maximum holding pressure for nanopores filled with condensed sealing molecules:  $\Delta P = 2\gamma \cos \theta / r$ ,

where  $\Delta P$  is the pore-entry pressure,  $\gamma$  is the liquid surface tension,  $\theta$  is the contact angle, and  $r$  is pore radius. When 2,2-dimethylbutane (DMB) is used as the sealing molecule in 1.5 nm alumina or silica pores, the estimated pressure that can push the liquid out of the pore is approximately 200 bar, given the surface tension of DMB is 15.7

mN·m<sup>-1</sup> (J. Chem. Eng. Data 2009, 54 (6) 1761) and assuming DMB completely wets the pore wall.

Table B1. Atomic EDS analysis for MCM-48-5A.

Element	5A region (points 4-6)	MCM-48 region (points 1-3)
Al	19.8	0.0
Si	22.3	31.4
O	49.6	68.6
Ca	3.5	0.0
Na	4.8	0.0

Table B2. BET area before and after MCM-48 coating.

Sample	BET area (m <sup>2</sup> /g)	% of reduction
5A zeolite beads	453	baseline
MCM-48-5A adsorbent	367	19

Table B3. Energy densities of sorbents at 25°C with loading pressures of 250 and 300 bar.

Material	Crystal density (g/mL)	Energy density at 250 bar		Energy Density at 300 bar	
		Volumetric (MJ/L)	Gravimetric (g CH <sub>4</sub> /g sorbent)	Volumetric (MJ/L)	Gravimetric (g CH <sub>4</sub> /g sorbent)
MOF-177	0.42	12.7	0.54	13.3	0.556
COF-102	0.42	13.0	0.56	13.5	0.578
COF-105-Eth-trans	0.26	13.2	0.91	13.9	0.962

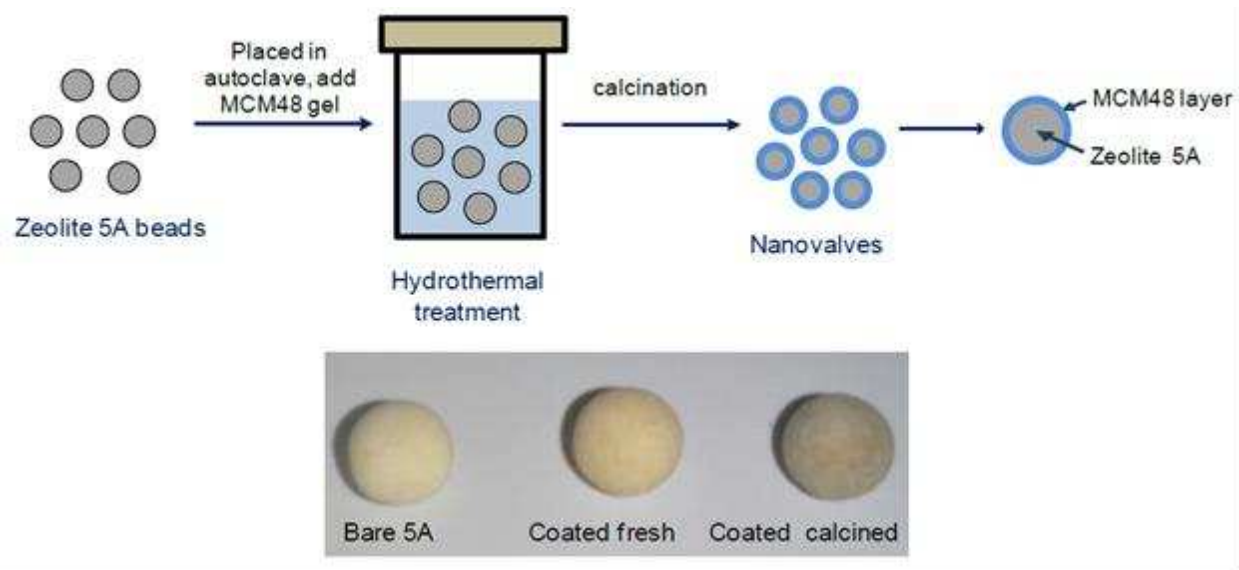


Figure B1. Diagram of coating procedure for MCM-48-5A adsorbent and pictures of samples.

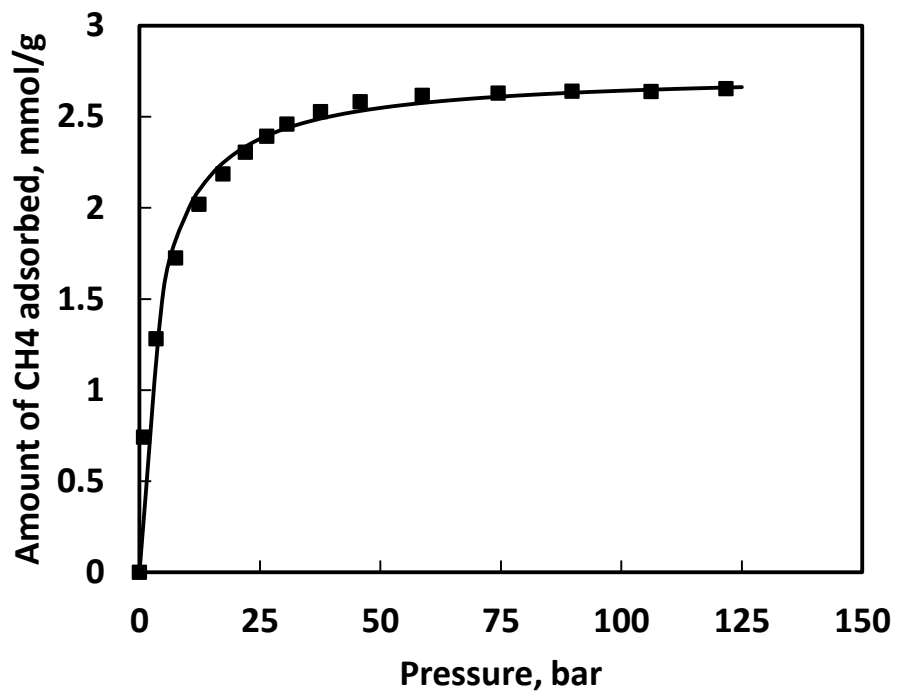


Figure B2. Adsorption isotherm of uncoated 5A zeolite beads at 20°C.

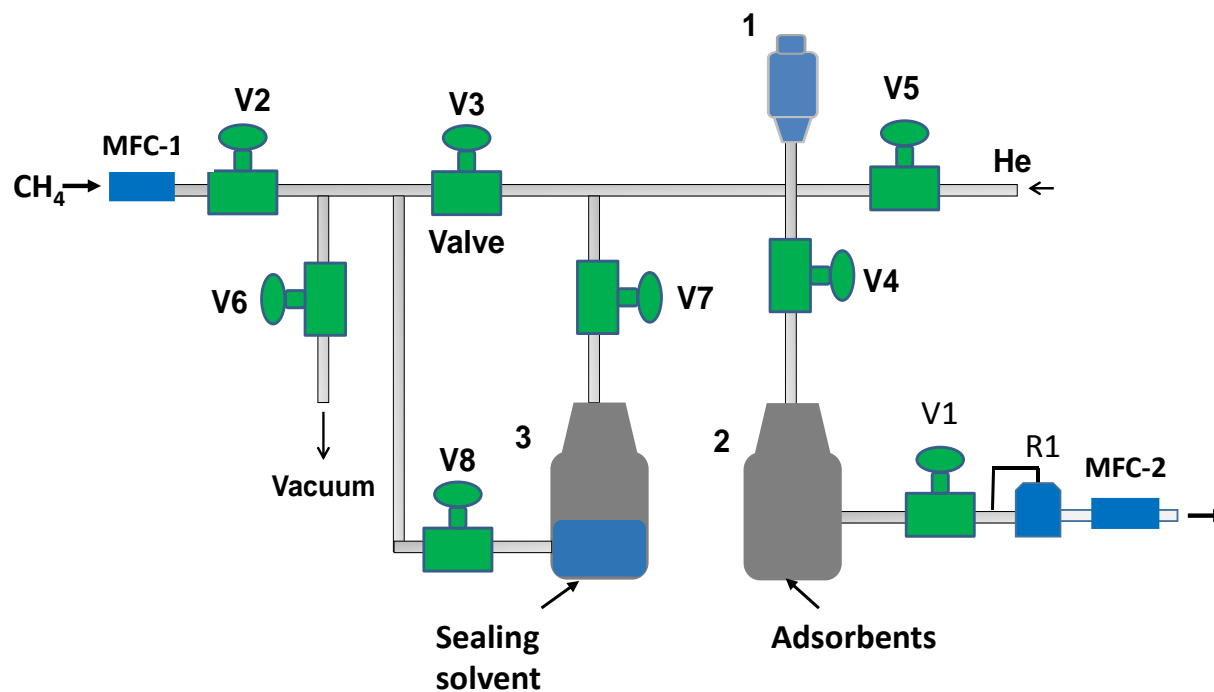


Figure B3. Nano-valved sorbent functioning testing system. 1-pressure transducer, 2-adsorption tank, 3-reference cell, MFC-mass flow controller, R1-back pressure regulator, V1-V8 valve.

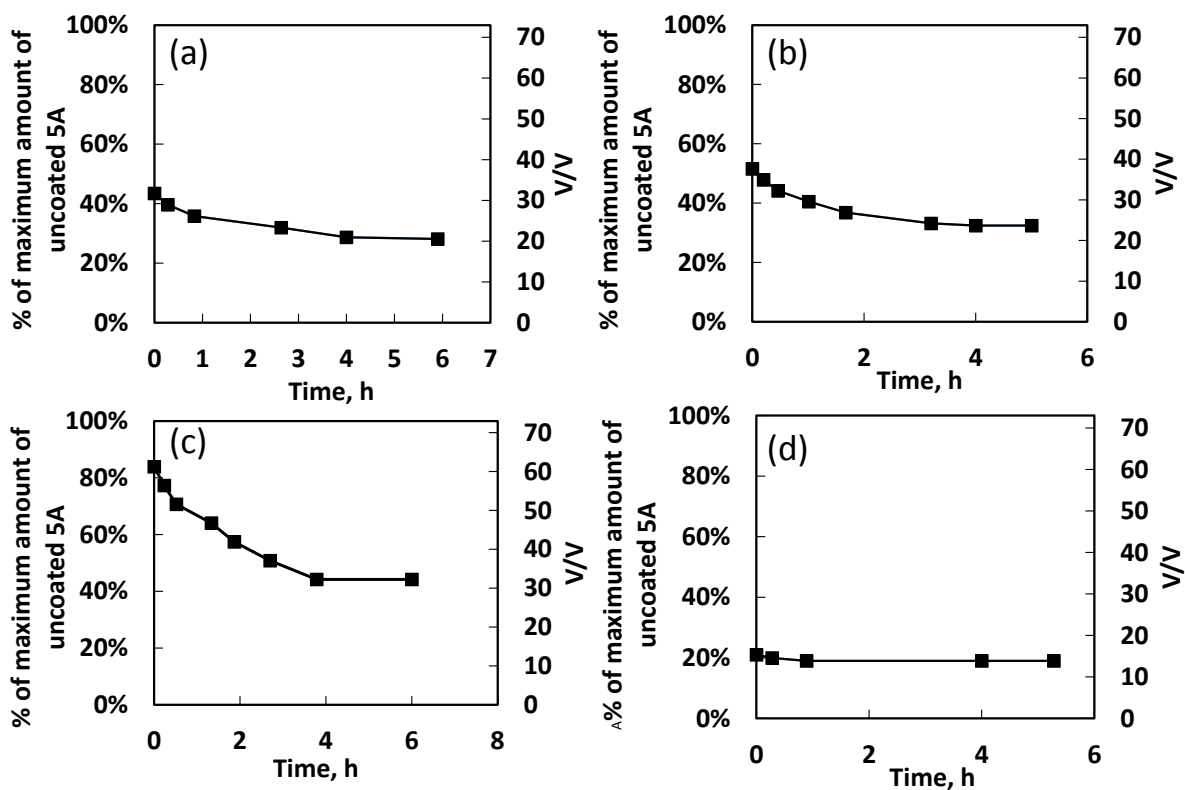


Figure B4. CH<sub>4</sub> storage test (loading pressure 50 bar, storage pressure 1bar) on MCM-48-5A adsorbent calcined at 350°C (a); calcined at 400°C (b); calcined at 450°C; uncoated 5A zeolite (d).

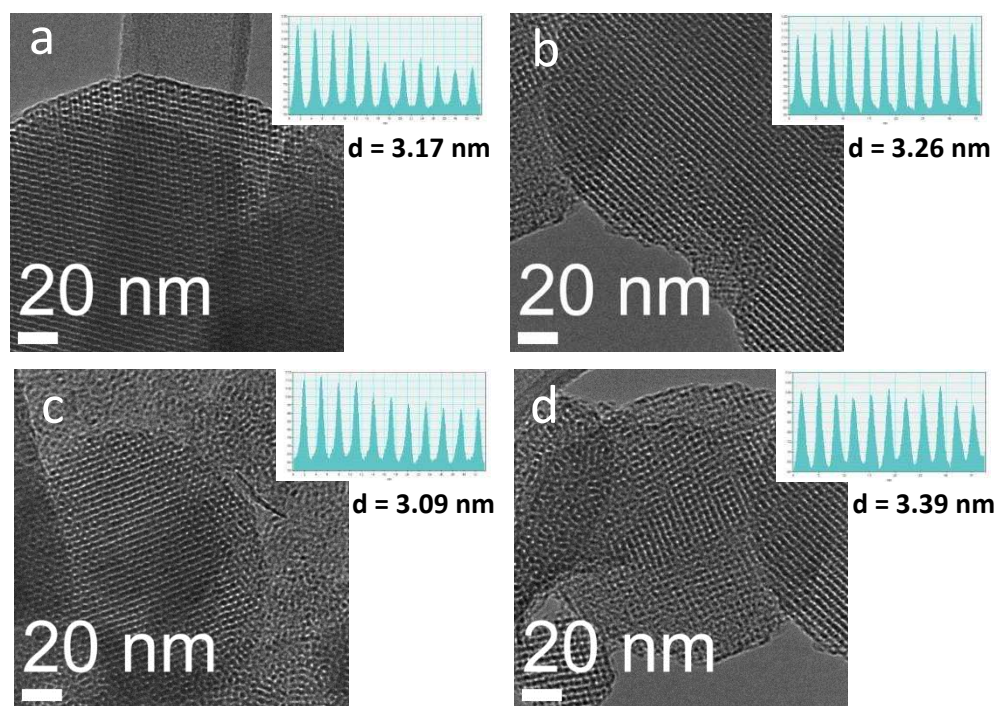


Figure B5. HRTEM images and pore sizes of MCM-48-5A adsorbents.

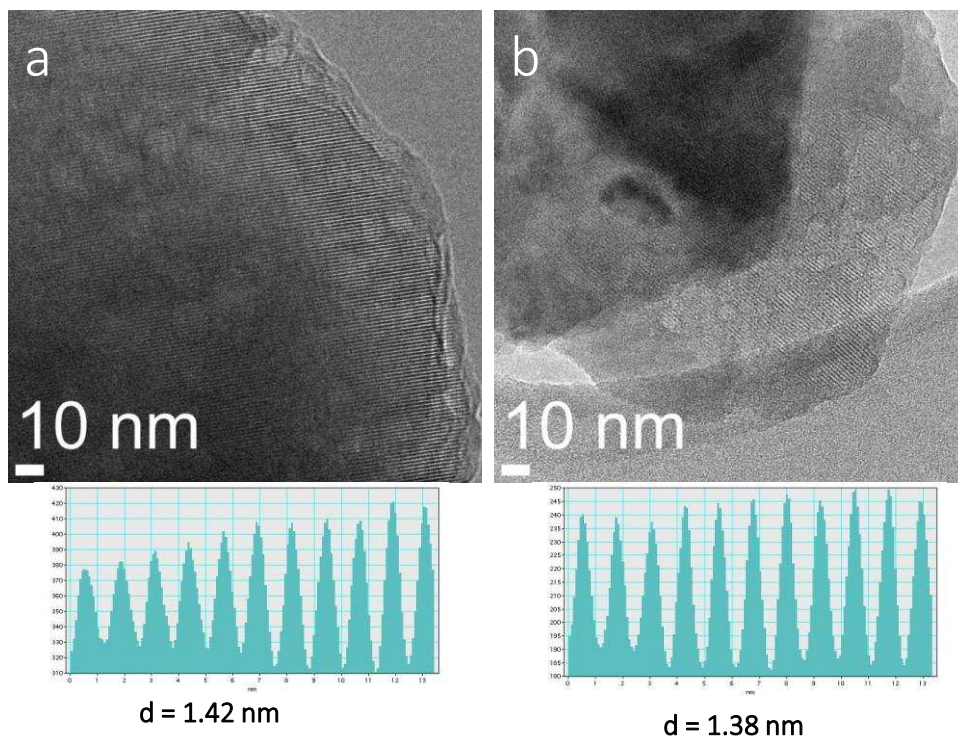


Figure B6. HRTEM images and pore sizes of MLD-MCM-48-5A adsorbents.